AFRL-AFOSR-VA-TR-2018-0375

Cyborgcell: Molecular-Nanoscale Circuits for Active Control of Cells

Charles Lieber
HARVARD COLLEGE PRESIDENT & FELLOWS OF

08/27/2018
Final Report

DISTRIBUTION A: Distribution approved for public release.

Air Force Research Laboratory
AF Office Of Scientific Research (AFOSR)/ RTB2
Arlington, Virginia 22203
Air Force Materiel Command

REPORT DOCUMENTATION PAGE

Form Approved
OMB No. 0704-0188

The public reporting burden for this collection of information is estimated to average 1 hour per response, including the time for reviewing instructions, searching existing data sources, gathering and maintaining the data needed, and completing and reviewing the collection of information. Send comments regarding this burden estimate or any other aspect of this collection of information, including suggestions for reducing the burden, to Department of Defense, Washington Headquarters Services, Directorate for Information Operations and Reports (0704-0188), 1215 Jefferson Davis Highway, Suite 1204, Arlington, VA 22202-4302. Respondents should be aware that notwithstanding any other provision of law, no person shall be subject to any penalty for failing to comply with a collection of information if it does not display a currently valid OMB control number.
PLEASE DO NOT RETURN YOUR FORM TO THE ABOVE ADDRESS.

1. REPORT DATE *(DD-MM-YYYY)*	2. REPORT TYPE	3. DATES COVERED *(From - To)*
08/27/2018	Final	9/15/2015-9/14/2018

4. TITLE AND SUBTITLE
Cyborgcell: Molecular-Nanoscale Circuits for Active Control of Cells

5a. CONTRACT NUMBER

5b. GRANT NUMBER
FA9550-15-1-0401

5c. PROGRAM ELEMENT NUMBER

5d. PROJECT NUMBER

5e. TASK NUMBER

5f. WORK UNIT NUMBER

6. AUTHOR(S)
Lieber, Charles M.

7. PERFORMING ORGANIZATION NAME(S) AND ADDRESS(ES)
President and Fellows of Harvard College
Richard A. and Susan F. Smith Campus Center, 1350 Massachusetts Avenue, Suite 600
Cambridge, Massachusetts 02138-3846

8. PERFORMING ORGANIZATION REPORT NUMBER

9. SPONSORING/MONITORING AGENCY NAME(S) AND ADDRESS(ES)
USAF, AFRL DUNS 143574726
Air Force Office of Scientific Research
875 North Randolph Street, Rm 3112
Arlington, VA 22203-1954

10. SPONSOR/MONITOR'S ACRONYM(S)

11. SPONSOR/MONITOR'S REPORT NUMBER(S)

12. DISTRIBUTION/AVAILABILITY STATEMENT
Approved for public release, distribution unlimited

13. SUPPLEMENTARY NOTES

14. ABSTRACT
The goal of this work is to develop molecular-nanoscale circuits that control cells via external radiation. We developed silicon nanowire probes as platform elements of these circuits and demonstrated their insertion into single cells followed by stimulation to elicit cell signaling, finally achieving a scalable, modular nanodevice platform capable of recording high-amplitude intracellular electrical signals in electrogenic cells. In parallel we developed a conformal deposition technique and site-selective deposition of polymers to modify probes, and an approach to decorate nanowires with heavy-metal-free quantum dot emitters that provide a strong, macroscopically addressable and reproducible nanoprobe emission signal.

15. SUBJECT TERMS
silicon nanowire probes, nano-bioelectronic interface, molecular-nanoscale circuit, cyborgcell, cell stimulation, cell signaling, nanodevice platform, probe internalization

16. SECURITY CLASSIFICATION OF:			17. LIMITATION OF ABSTRACT	18. NUMBER OF PAGES	19a. NAME OF RESPONSIBLE PERSON
a. REPORT	b. ABSTRACT	c. THIS PAGE			Charles M. Lieber
U	U	U	UU	28	19b. TELEPHONE NUMBER *(Include area code)* 617-496-3169

DISTRIBUTION A: Distribution approved for public release.

Standard Form 298 (Rev. 8/98)
Prescribed by ANSI Std. Z39.18

INSTRUCTIONS FOR COMPLETING SF 298

1. REPORT DATE. Full publication date, including day, month, if available. Must cite at least the year and be Year 2000 compliant, e.g. 30-06-1998; xx-06-1998; xx-xx-1998.

2. REPORT TYPE. State the type of report, such as final, technical, interim, memorandum, master's thesis, progress, quarterly, research, special, group study, etc.

3. DATE COVERED. Indicate the time during which the work was performed and the report was written, e.g., Jun 1997 - Jun 1998; 1-10 Jun 1996; May - Nov 1998; Nov 1998.

4. TITLE. Enter title and subtitle with volume number and part number, if applicable. On classified documents, enter the title classification in parentheses.

5a. CONTRACT NUMBER. Enter all contract numbers as they appear in the report, e.g. F33315-86-C-5169.

5b. GRANT NUMBER. Enter all grant numbers as they appear in the report. e.g. AFOSR-82-1234.

5c. PROGRAM ELEMENT NUMBER. Enter all program element numbers as they appear in the report, e.g. 61101A.

5e. TASK NUMBER. Enter all task numbers as they appear in the report, e.g. 05; RF0330201; T4112.

5f. WORK UNIT NUMBER. Enter all work unit numbers as they appear in the report, e.g. 001; AFAPL30480105.

6. AUTHOR(S). Enter name(s) of person(s) responsible for writing the report, performing the research, or credited with the content of the report. The form of entry is the last name, first name, middle initial, and additional qualifiers separated by commas, e.g. Smith, Richard, J, Jr.

7. PERFORMING ORGANIZATION NAME(S) AND ADDRESS(ES). Self-explanatory.

8. PERFORMING ORGANIZATION REPORT NUMBER. Enter all unique alphanumeric report numbers assigned by the performing organization, e.g. BRL-1234; AFWL-TR-85-4017-Vol-21-PT-2.

9. SPONSORING/MONITORING AGENCY NAME(S) AND ADDRESS(ES). Enter the name and address of the organization(s) financially responsible for and monitoring the work.

10. SPONSOR/MONITOR'S ACRONYM(S). Enter, if available, e.g. BRL, ARDEC, NADC.

11. SPONSOR/MONITOR'S REPORT NUMBER(S). Enter report number as assigned by the sponsoring/ monitoring agency, if available, e.g. BRL-TR-829; -215.

12. DISTRIBUTION/AVAILABILITY STATEMENT. Use agency-mandated availability statements to indicate the public availability or distribution limitations of the report. If additional limitations/ restrictions or special markings are indicated, follow agency authorization procedures, e.g. RD/FRD, PROPIN, ITAR, etc. Include copyright information.

13. SUPPLEMENTARY NOTES. Enter information not included elsewhere such as: prepared in cooperation with; translation of; report supersedes; old edition number, etc.

14. ABSTRACT. A brief (approximately 200 words) factual summary of the most significant information.

15. SUBJECT TERMS. Key words or phrases identifying major concepts in the report.

16. SECURITY CLASSIFICATION. Enter security classification in accordance with security classification regulations, e.g. U, C, S, etc. If this form contains classified information, stamp classification level on the top and bottom of this page.

17. LIMITATION OF ABSTRACT. This block must be completed to assign a distribution limitation to the abstract. Enter UU (Unclassified Unlimited) or SAR (Same as Report). An entry in this block is necessary if the abstract is to be limited.

DISTRIBUTION A: Distribution approved for public release.

Final Performance Report – Years 1-3

Project Title:	Cyborgcell: Molecular-Nanoscale Circuits for Active Control of Cells
Award Number:	FA9550-15-1-0401
Reporting Period:	09/15/2015 - 09/14/2018
Program Manager:	Dr. Patrick Bradshaw AFOSR/RTB2 875 North Randolph Street 4027 Arlington, VA 22203 E-mail: patrick.bradshaw.3@us.af.mil Phone: (703) 588-8492
Principal Investigators:	Professor Charles M. Lieber Professor Daniel G. Nocera Department of Chemistry and Chemical Biology Harvard University 12 Oxford Street Cambridge, MA 02138 E-mail: cml@cmliris.harvard.edu, dnocera@fas.harvard.edu Phone (Lieber): (617) 496-3169 Phone (Nocera): (617) 495-8904

DISTRIBUTION A: Distribution approved for public release.

AFOSR Final Performance Report – Years 1-3

"Cyborgcell: Molecular-Nanoscale Circuits for Active Control of Cells"

PIs: Professor Charles M. Lieber, Professor Daniel G. Nocera

Project Description and Objectives. The overall goal of our proposed project is the development of a novel molecular-nanoscale device that actively controls the behavior of cells and ultimately cellular networks. The development of synthetic molecular electronic circuits, which can be inserted into single cells and modulate the cellular function in a controlled manner, has not been reported, although such circuits could open up a new frontier in both fundamental and applied research field focused on understanding and controlling cellular systems. Our effort spans the fields of nanoscience, chemistry, biology, material science and photonics to achieve this broad goal with a focus on five integrated aims. (1) The design, synthesis and characterization of a basic nanowire nanodevice platform that allows wavelength-specific absorption and transfer of optical energy and/or optically-driven charge separation. Integrated theoretical simulations and experimental studies are used to optimize the properties of the nanowire circuit elements. (2) Molecular functionalization of nanowire elements for controlled cellular entry, including coupling of cell-penetrating peptides to nanowire surfaces. Single device/circuit-level assays are carried out to characterize and optimize biochemically-driven internalization and bio-stability of the functionalized nanowires. (3) Design, synthesis and characterization of a suite of molecular device elements that can be selectively coupled to the nanowire components to build molecular-nanoscale circuits. (4) Selective coupling of the specific classes of molecular devices to nanowire antenna elements required for transport of photons or charges. (5) Investigation of the fully assembled molecular-nanoscale circuits for controlled internalization and subsequent optical control of cellular function. The goal of the proposed research effort is to yield significant advances at the frontiers of molecular electronics with the creation of new classes of wireless molecular-nanoscale circuits, and demonstration that these circuits can be integrated with and subsequently control the function of living cells.

Summary. During the first year of the project, the Lieber team successfully developed silicon nanowire probes as a nano-bioelectric interfacial platform for the development of synthetic molecular electronic circuits, while the Nocera team focused on development of a conformal deposition technique to modify silicon nanowire probes and development of site-selective deposition of polymers with and without active molecular species. In the second year, the Lieber team extended its work on these silicon nanowire probes to enable them to be inserted into a single cell and then to stimulate the cell to elicit a cell-signaling event, while the Nocera team conducted studies on the integration of preliminary device architectures with neuronal cells, honing tip-selective deposition methods and exploring new avenues to incorporate active molecular species onto devices using mesoporous silica. In Year 3 the Nocera team worked on understanding and controlling the diffusion of embedded molecular species into aqueous media, developing strategies to enhance the encapsulation of the molecular species and adhesion of polymer layers to substrate. They have also developed a new platform for the decoration of nanowires with heavy-metal-free quantum dot emitters that provide a strong nanoprobe emission signal that is macroscopically addressable and reproducible. In parallel, the Lieber team worked on developing a scalable, modular nanodevice platform capable of recording high amplitude intracellular electrical signals in a variety of electrogenic cells as well as understanding the influence of device geometry on promoting internalization. These research accomplishments are described in detail below.

DISTRIBUTION A: Distribution approved for public release.

Accomplishments.

Objective 1: *To design, synthesize and characterize a nanowire nanodevice platform that allows for wavelength-specific absorption and transfer of optical energy and/or optically driven charge separation.*

(Nocera team – Year 1) Efforts on this objective exploited the Nocera team's expertise in electrochemical deposition to pursue synthesis of semiconductor integrated multi-segmented coaxial nanowires. Significant progress was made on the synthesis and characterization of several types of metal, oxide, and organic and inorganic semiconductor functionalized silicon wires. Vertically oriented silicon wires were obtained from the Lieber team, which employed top-down microfabrication to produce the nanowire array. Electrochemical modification of these nanowire arrays was performed in a Teflon cell with a conventional three-electrode (Ag/AgCl reference, Pt counter, Si working) set-up. Parameters for electrodeposition of specific materials were optimized individually by using different electrolyte solutions, material precursors, deposition potentials, and potential profiles to furnish reproducible processes for the synthesis of conformal coatings around silicon wires. Furthermore, sequential deposition of metals and semiconductors can yield multi-segmented coaxial nanowires. In a typical experiment, metal layers of Ni and Au were deposited at -900 mV (vs. Ag/AgCl) from nickel sulfamate and gold cyanide solutions, respectively. Conductive polymer layers of poly(3,4ethylenedioxythiophene) (PEDOT) and polypyrrole (PPy) were electropolymerized at +1000 mV (vs. Ag/AgCl) from solutions of 3,4-ethylenedioxy-thiophene (EDOT) and pyrrole in 0.1 M $LiClO_4$, respectively. CdSe, an inorganic semiconductor material, was deposited via simultaneous co-electrodeposition of Cd and Se atoms via cyclic voltammetry (cycling between -387 and -787 mV vs. Hg/Hg_2Cl_2). Electron microscope images of some nanowires with varying conformal coatings (Au, Ni, PEDOT, CdSe) are presented in **Fig. 1**.

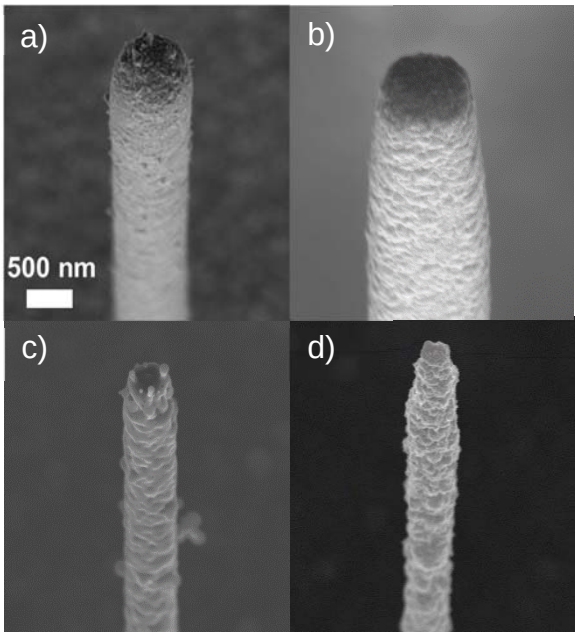

Fig. 1. Electron microscope images of silicon nanowires coated with a) Au b) Ni c) PEDOT and d) CdSe shell layers.

Further modification of the nanowires can be accomplished with conventional nanofabrication techniques such as reactive ion etching (RIE). In an optimized RIE process using directional argon plasma, the tips of the wires can be anisotropically etched. **Fig. 2a-b** show nanowires after etching with RIE, in which argon plasma has directionally removed the top portion of the nanowires, resulting in tip-cleaned, core-shell

DISTRIBUTION A: Distribution approved for public release.

nanowire architectures. This method provides another handle with which to control site-selective functionalization and structural design of the silicon nanowires.

Using this methodology, we created more complex core-shell nanowire structures through the use of sacrificial layers that can be selectively etched. For example, sequential, alternating depositions of nickel and gold layers yield the multi-shell structure shown in **Fig. 2c** post-tip etching. Selective wet etching of nickel then yields a core-shell structure with two gold shells surrounding a silicon nanowire as shown in **Fig. 2d**.

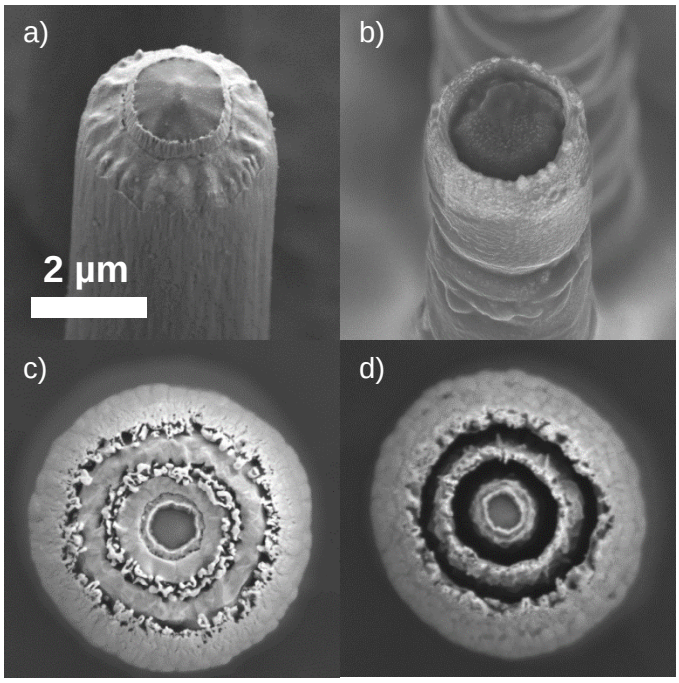

Fig. 2. Electron microscope images of a) Ni and b) PPy coated silicon nanowires after argon plasma RIE etching. RIE-etched Ni-Au-Ni-Au core shell silicon nanowires c) before and d) after wet etching of sacrificial Ni layers.

With the methodology used to prepare the nanowires depicted in **Figs. 1 and 2**, it is possible to fabricate functional coaxial nanowire devices as we are now able deposit various layers of semiconductors and metals onto the same wire. Most of the deposition parameters are optimized to achieve precise control over the thickness of each layer. A natural next step is to fabricate core-shell type nanowires with p-type Si as the core and electrodeposited n-type CdSe as the shell with a metal electrode on top. Such a design would allow measurement of current-voltage characteristics and the photoresponse of nanodevices for future applications.

Objective 2: ***To develop molecular functionalization for controlled cellular entry such as selective coupling of cell-penetrating peptides to the nanowire components.***

(Lieber team – Year 1) A key component of the proposed studies is to exploit well-defined biological internalization mechanisms to enable controlled entry of nanowire circuits into cells. Biomimetic surface modification of nanodevices is a key approach for interfacing nanomaterial-based devices with biological systems. Appropriate surface modification allows the presentation of specific biochemical ligands that can interact with appropriate cellular receptors to enable specific cell type targeting, cellular internalization, and activation of biological pathways.[1] Though initial progress has been made,[2-5], creation of stable, intracellular bio-nano interfaces remains challenging. For example, nanoscale sensing elements made with silicon nanowire (Si NW) functionalized with a lipid bilayer have been internalized across the cardiac cell membrane and recorded action potentials without compromising cell viability.[2,4]

Additionally, vertical NW arrays on cultured cells have been shown to deliver biomolecules to the cytoplasm by means of gravity and/or adhesive force driven internalization.[6-9] Also, electroporation has been used to achieve transient access to intracellular action potentials.[5] In another approach, chemical treatment such as a polar organic solvent (e.g. DMSO) of the cell membrane was used to render the mechanical properties of cell membrane more porous/flexible to more easily internalize NW.[10] However, these methods offer only transient access to the interior of the cell and/or are not effective for all cell types, in particular neurons. Intracellular nano-bio interfacing requires the development of a robust, general strategy for internalization of nanoscale sensors. Below we describe our efforts in this regard using cell-penetrating peptide and adenovirus modification.

Cell-penetrating peptide modification. NW-based sensors are comparable in length to large macromolecules, viruses, and proteins, which use intrinsic cellular machinery to cross the cell membrane. A new approach developed in this project adopts this strategy, using biomimetic functionalization to induce cellular uptake of nanodevices. Trans-activating transcriptional factor (TAT) for human immunodeficiency virus-1 (HIV-1) is a well-known cell penetrating peptide (CPP)[11] which is effective at transporting varieties of small molecules,[12] nucleic acids,[13,14] proteins,[15,16] and submicron particles[17]

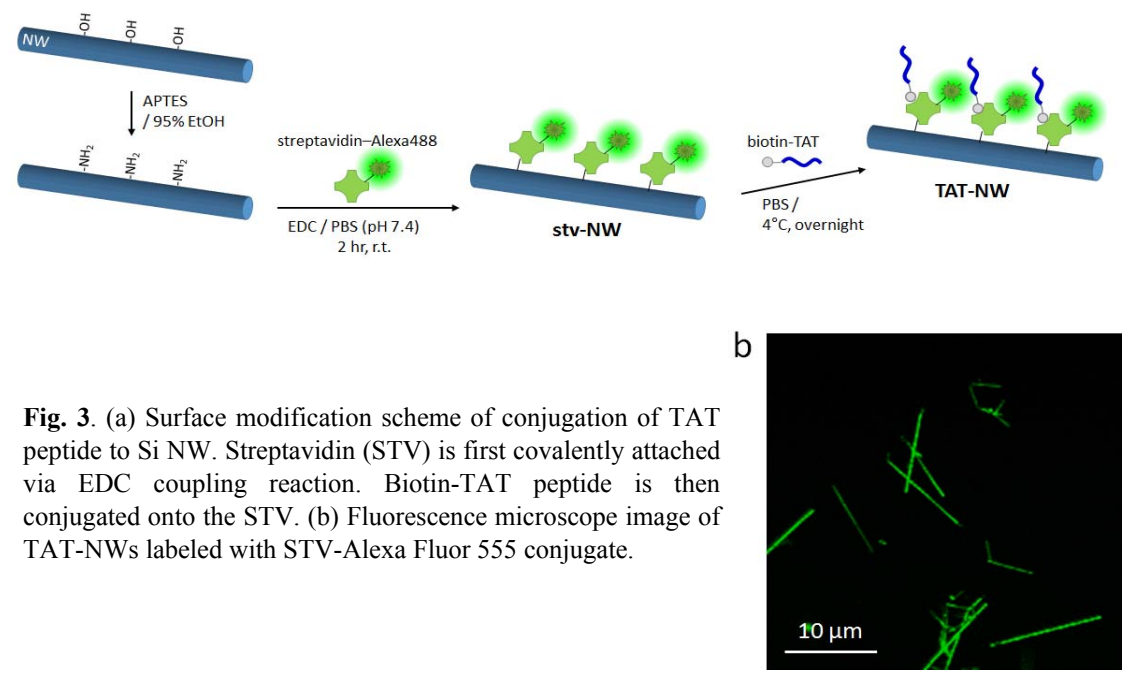

Fig. 3. (a) Surface modification scheme of conjugation of TAT peptide to Si NW. Streptavidin (STV) is first covalently attached via EDC coupling reaction. Biotin-TAT peptide is then conjugated onto the STV. (b) Fluorescence microscope image of TAT-NWs labeled with STV-Alexa Fluor 555 conjugate.

across the membrane of primary cells (e.g. neuron) and immortalized tumor cell lines. The membrane-penetrating properties of this TAT peptide were harnessed by conjugating it to the chemically modified surface of a Si NW (**Fig. 3a**): First, Si NWs (n-doped, 80 nm in diameter and ~10 µm in length) were synthesized by the gold nanocluster catalyzed vapor-liquid-solid method, for which the growth conditions, mechanism, and characterization are well-established.[18] Second, the NWs on the growth substrate were modified with (3-aminopropyl)-triethoxysilane (APTES) to yield a primary amine-terminated monolayer. Third, Alexa Fluor 555 labeled streptavidin (STV) was covalently coupled to NWs using 1-ethyl-3-(3-(dimethylamino)propyl) carbodiimide (EDC). Fourth, the STV-modified NW (STV-NW) substrate was incubated in biotin-TAT solution for binding. The resulting TAT-conjugated Si NWs (TAT-NWs) were detached from the substrate by brief sonication. A representative fluorescent image of TAT-NW dispersed

DISTRIBUTION A: Distribution approved for public release.

on a glass substrate is shown in **Fig. 3b**. The homogeneous fluorescence along the NW surface indicates that conjugation of STV and TAT is uniform.

Neuronal internalization of TAT modified Si NW. Internalization of TAT-modified Si NW (TAT-NW) into neurons was confirmed with confocal microscopy. First, dispersed TAT-NWs are delivered to a culture of mouse hippocampal neurons. The NW-cell mixture is then incubated for a fixed time (e.g. 20 hrs), and confocal microscopy used to analyze the positions of NWs with respect to the cell membrane. At the chosen time points, confocal microscopy images are recorded at different distances relative to the substrate surface with distinct fluorescent labels for the NWs, cell membranes, and cell nuclei. During image processing, NW positions are analyzed relative to the membrane surface in either a 3D top- or cross-sectional view.

Fig. 4a shows the overview of our strategy using TAT-NW for internalization into neuron and **Fig. 4b** shows the internalization schematics and the actual confocal microscope images in a top-down z-stack view and side z-section view, where TAT-NWs (5 µg) were dispersed and incubated with the mouse embryonic hippocampus neuron culture (two weeks after cell seeding) for 20 hrs at 37 ºC. As a control, STV-NWs without TAT modification were dispersed in a similar manner on a separate neuron culture and incubated (**Fig. 4c**). For confocal imaging, cells were fixed and fluorescently labeled with WGA-Alexa Fluor 594 for membrane staining and Hoechst 33258 for nuclei staining. The z-section views of confocal images show that TAT-NW interact with the neuronal membrane and facilitate spontaneous internalization without affecting neuronal membrane integrity, while the control STV-NW was not internalized, remaining on the cell surface.[19]

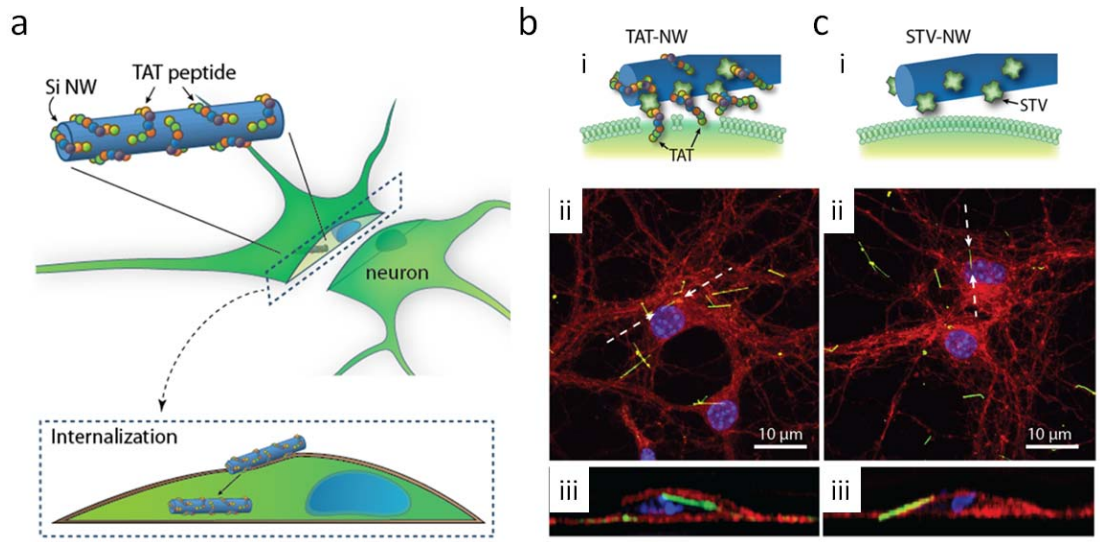

Fig. 4. (a) Schematic of internalization of TAT peptide modified Si NW into neuron. (b) TAT-NW and (c) STV-NW interactions with the hippocampus neuronal membrane; (i) schematics, (ii) confocal microscope z-stack image, and (iii) z-section image along the white dashed line in (ii). Z-stack images consist of 29 individual images with 0.5 µm slice thickness. Red: cell membrane (WGA-Alexa 597); green: NWs (Alexa 555); blue: nucleus (Hoechst 33258).

In-situ confocal imaging of TAT-NW internalization into hippocampus neuron and dorsal root ganglia (DRG) neuron. To better understand the dynamics of the TAT-NW internalization process, we carried out in-situ live-cell confocal imaging. To maintain cell viability during the imaging process, the imaging chamber was designed for an upright confocal microscope, utilizing a Petri dish with a hole in

the top lid for access of an objective lens and with x-y location markers on the bottom lid for fast and exact positioning of the target cell during consecutive imaging sessions. The chamber was placed on a heating plate to maintain a constant temperature of 37 ºC. To image the dynamics of TAT-NW interfacing to and penetrating the neuronal membrane, TAT-NW (5 µg) was placed on a hippocampal neuron culture and incubated for 30 min at 37 ºC, during which NWs were allowed to deposit onto the cell surface. After that, the culture was placed in the imaging chamber and the cells imaged every ten minutes with the confocal microscope for 1-2 hours. Representative images of TAT-NW being internalized into hippocampal and DRG neurons are shown in **Fig. 5a,b**, where several key points are demonstrated. First, TAT-NWs begin to cross the neuronal cell membrane within only 10-20 min of initial attachment. Second, internalization is complete for the characterized NWs within 30-40 min. Third, STV-NWs maintain constant positions on the cell membrane indicating that there is no internalization over this same period of time (**Fig. 5c**). Fourth, TAT-NW can be internalized into other primary neuron types, such as DRG cells, suggesting that this modification scheme has potential as a general strategy for internalization of NW

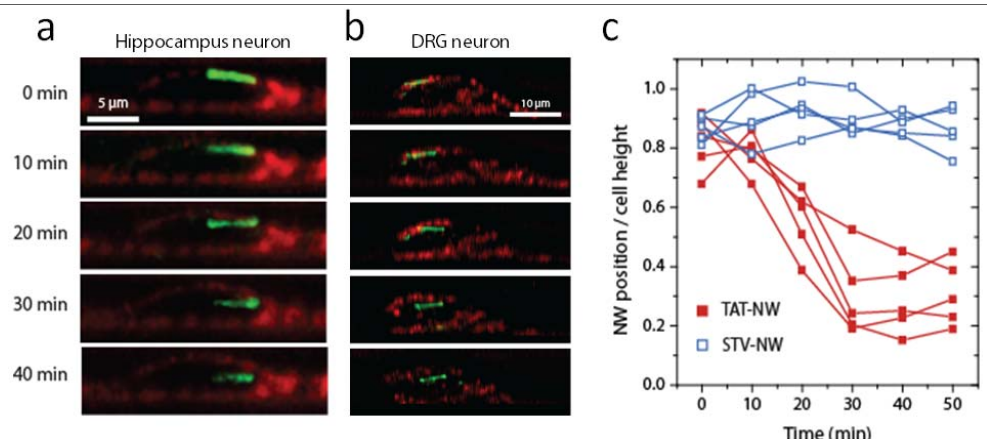

Fig. 5. Real-time imaging of TAT-NW internalization. Temporal cross-section confocal images of TAT-NW interfaced with (a) hippocampus neuron and (b) dorsal root ganglia (DRG) neuron. Neuronal membrane is stained with WGA-Alexa 594 (red) and TAT-NW is stained with Alexa 555 (green). (c) Temporal changes of the relative positions of TAT-NWs and STV-NWs (control) from the bottom of cell; N = 5 for each NW type.

devices Last, following internalization we monitored cell viability using calcein-AM dye and found 97% fluorescence intensity was retained after 3 h, indicating that NW internalization has a minimal influence on cell activity/viability on this time scale.[19]

Adenovirus modification of Si NW. As an alternative approach to achieve transmembrane penetration, since viral particles are an effective cell-penetrating agent, we modified the Si NW surface for conjugation of adenovirus (ADV). ADV is well-known virus, particles of which range from 80 to 100 nm, with an icosahedral capsid containing double-stranded DNAs. ADV has been studied widely as a vehicle for gene transfection in which internalization into the target cell occurs via receptor-mediated endocytosis.[20] The receptors required are coxsackievirus and adenovirus receptor (CAR) and αβ integrin co-receptor, which are already expressed in most neurons,[21] making ADV a good transfection agent for the genetic engineering of neurons in, for example, optogenetics[22] and a promising candidate virus to couple to our Si NW devices.

To conjugate ADV on Si NW (**Fig. 6a**), Si NW was synthesized by the vapor-liquid-solid method with 80 nm gold nanoparticles as a catalyst and modified with APTES to yield primary amine-modified nanowire surface in 95% ethanol. Second, the modified Si NWs were further reacted with disuccinimidyl carbonate (DSC) in dimethylsulfoxide (DMSO) for 24 hrs which transforms the Si NW surface to expose

DISTRIBUTION A: Distribution approved for public release.

succinimide, a well-known linker forming a covalent bond with primary amine on the target molecule. Third, a concentrated solution of ADVs (~10^{11} particle/mL) was dispersed on the succinimide-modified Si NW for 1 hour in phosphate buffered saline (PBS) solution. The ADV capsid has ~18,000 lysine and

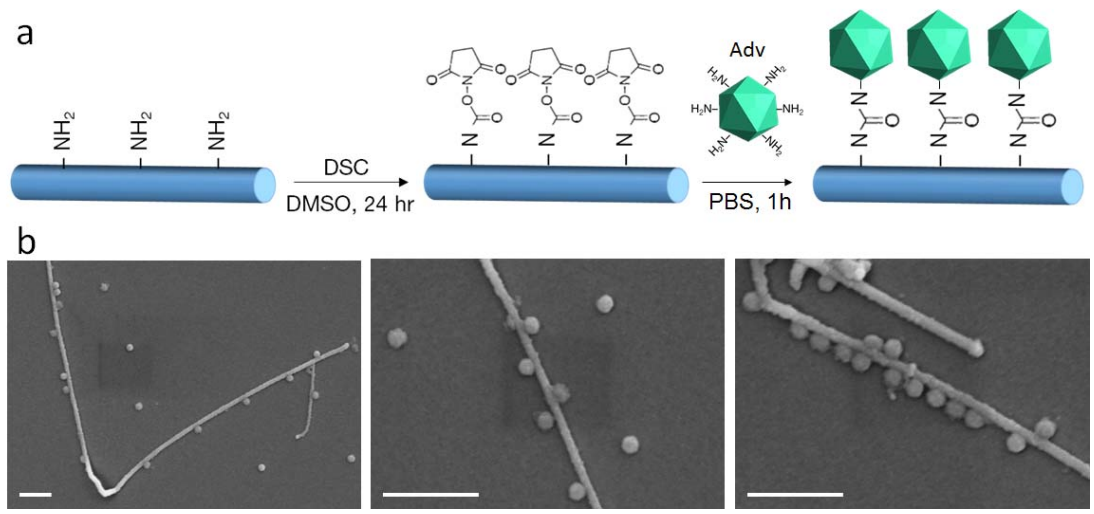

Fig. 6. (a) Two-step surface modification scheme for ADV conjugation to Si NW. APTES-modified NWs are firstly reacted with DSC to modify the surface with succinimide and then further reacted with ADV for amine mediated conjugation to NW. (b) Scanning electron microscope (SEM) images of ADV conjugated Si NW (ADV-NW). Scale bar = 500 nm. Acronyms correspond to the following chemicals, DSC: disuccinimide carbonate, DMSO: dimethylsulfoxide, ADV: adenovirus, PBS: phosphate buffered saline.

arginine residues in total,[23] which act as binding sites for the DSC-modified Si NW and eventually yield ADV and Si NW conjugates (ADV-NW). Scanning electron microscope (SEM) images show the representative ADV-NW conjugates (Fig. 6b), where 10-20 ADV particles are observed on each NW.

Design and fabrication of nanodevices for internalization of Si NW. We designed and fabricated a Si NW based sensor based on our previous work. This nanodevice was designed as a free-standing probe with input/output to a computer, and can be mounted on a micromanipulator for measurements on a target cell with ~100 nm spatial resolution. A kinked Si NW was used at the tip of the probe, which was synthesized with n-type Si NW with controlled n-doping to have an n-type/intrinsic/n-type (n/i/n) axial junction at the tip of the kink (**Fig. 7**).[24] This n/i/n junction was designed to work as a field effect transistor (FET) sensing element for the detection of intracellular signals such as changes in Ca^{2+} concentration. Fabrication of the free-standing probe is shown schematically in **Fig. 8a**. The base of the probe is fabricated through photolithography on a silicon wafer in the following sequence; step 1: Ni or Al sacrificial layer, step 2: polymeric probe base with SU-8, and step 3: gold electrode layer for electric connection. After that, another coat of SU-8 polymer is added (step 4), kinked Si NWs deposited (step 5) and the additional layers of gold added to make contact to the nanowire for electrical readout. (step 6). The electric passivation

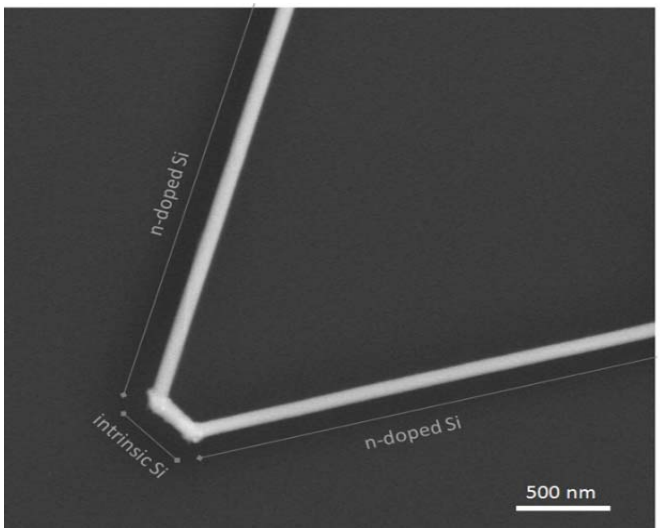

Fig. 7. SEM image of kinked Si NW with an n-type/intrinsic/n-type (n/i/n) axial junction at the tip of the kink.

DISTRIBUTION A: Distribution approved for public release.

layer with SU-8 polymer (step 7) was then deposited by electron beam lithography. Finally, an additional SU-8 polymer layer is placed on the probe base to electrically passivate the remainder of the probe (step 8). The completed probe is released from the silicon wafer by etching the sacrificial layer and dried (**Fig. 8b**). **Fig. 8c** shows the assembly procedure of the probe on a printed circuit board (PCB). The assembled probe is mounted on the micromanipulator of an upright microscope and ready to use for an internalization test. Devices can be fabricated in parallel, and 10–20 probes were fabricated in two weeks. This free-standing probe works similarly to the conventional patch clamp system in targeting and manipulating the cell, but shows better spatial precision due to the kinked Si NW tip, which has a sensitive region of ~200 nm.

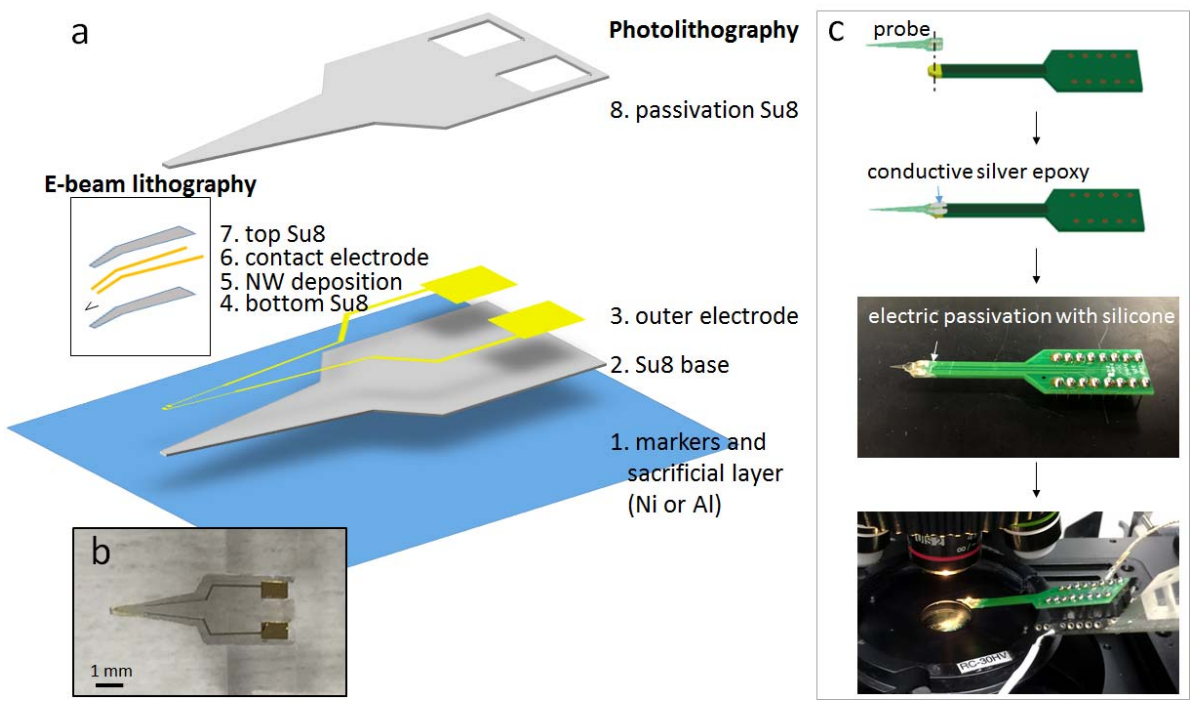

Fig. 8. Fabrication and assembly of free-standing Si NW probe for cell internalization. (a) Schematic of probe fabrication showing fabrication steps using photolithography and electron-beam lithography techniques. (b) A representative picture of the completed probe after lift-off from the silicon wafer. (c) Assembly of the probe on the printed circuit board (PCB). The probe was glued down on the PCB and electrically connected with silver epoxy. The electric parts of the PCB and the probe were then passivated with silicone and mounted on the micromanipulator of an upright microscope.

Nanodevice internalization into DRG neurons. Si NW device internalization into a DRG neuron was demonstrated by using the free-standing probe set-up modified with TAT peptide. The probe was brought into proximity with the target DRG neuron and the internalization process monitored using confocal microscopy (**Fig. 9**). DRG neurons were cultured 5-7 days and the cell culture tilted 60-80º from the bottom to achieve a side view of cells under the microscope. For fluorescent confocal imaging, the cells were stained with WGA-Alexa Fluor 594 and the Si NW and probe with Alexa Fluor 555 dye. The kinked Si NW was positioned on the cell membrane until the probe was stationary (**Fig. 9**, 0-5 min), then slight force was applied to push the probe into the cell (**Fig. 9**, 10-13 min). Complete internalization of NW was observed after 16 min.

DISTRIBUTION A: Distribution approved for public release.

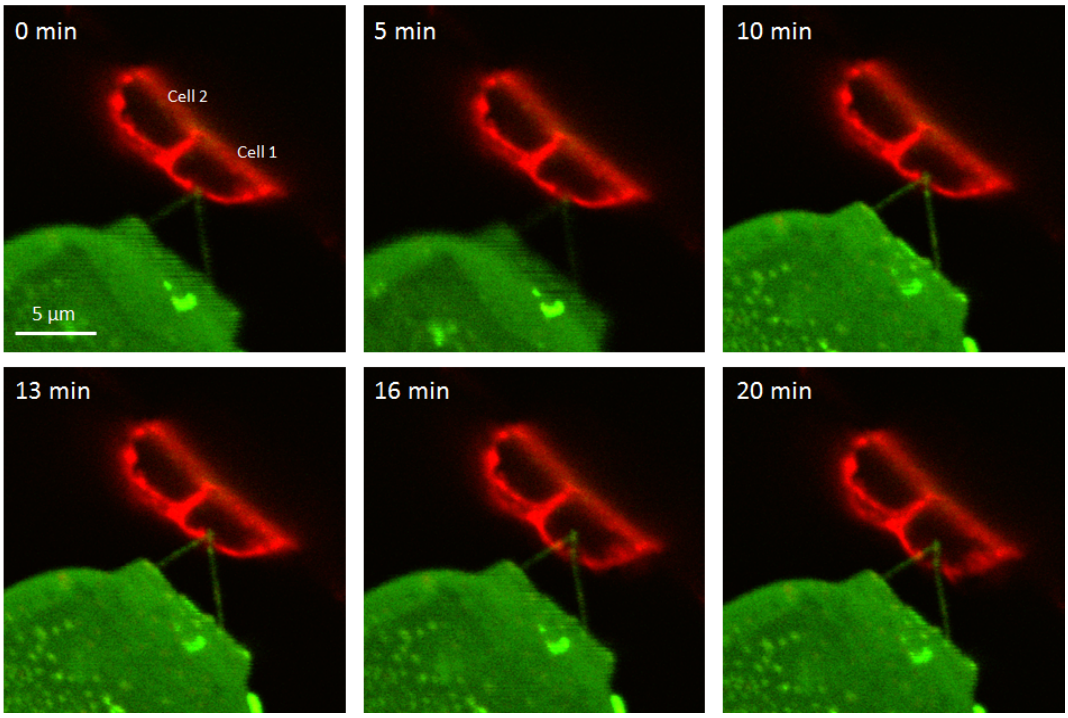

Fig. 9. Time series of fluorescent confocal images of a TAT conjugated Si NW probe being internalized into DRG neuron. Each image consists of 5 z-stack images with 0.5 µm slice thickness. Red: cell membrane (WGA-Alexa 597); green: NWs (Alexa 555).

Overcoming this technical challenge allows us to focus on electrical measurement of membrane potential and its change with electrical/chemical stimulation, which will be utilized for internalization of the molecular devices originally proposed.

Device design for controlled cell entry. (Nocera team – Year 2) We previously developed the synthesis of silicon nanowires with sulforhodamine B, a fluorescent dye, loaded into polymer-functionalized tips[25]. A novel, more efficient pathway to the same wire architecture is detailed under Objective (3). Images of the resulting wires are presented in **Fig. 10**. We have begun to investigate the cellular entry mechanisms of this prototypical device design, displaying the wire nanostructures.

The Lieber team has demonstrated in parallel work that freestanding, bare silicon nanowires grafted with cell-penetrating peptides can be internalized by cells.[19] We applied a similar approach to the functionalized nanowire device architecture shown in **Fig. 10**. The nanowires were labeled with a streptavidin-Alexa Fluor 405 dye using 1-ethyl-3-(3-(dimethylamino)propyl) carbodiimide (EDC) conjugation chemistry. A biotin-labeled trans-activating transcriptional activator (TAT) cell-penetrating peptide was subsequently conjugated to streptavidin, allowing the nanowire devices to be modified with a surface layer of TAT cell-penetrating peptide and a fluorescent dye with fluorescence distinguishable from that of the encapsulated sulforhodamine B at the tip of the nanowire.

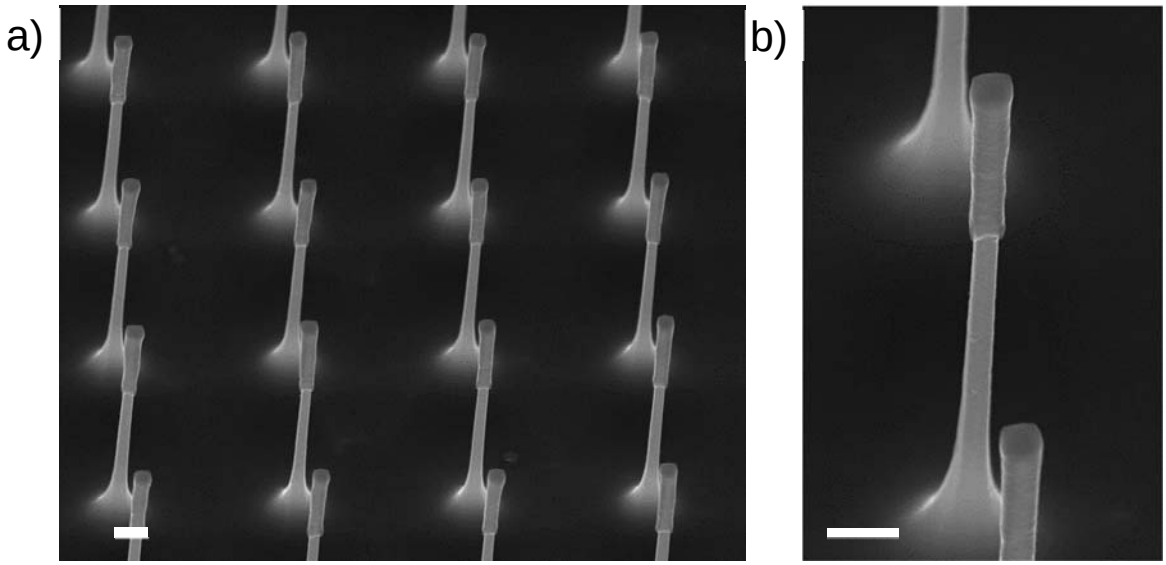

Fig. 10. a) Electron microscope image of silicon nanowires with sulforhodamine B loaded polypyrrole deposited at the tips. b) Zoomed-in images of nanowires in a). Scale bars 1 μm.

Hippocampal neurons were digested and collected from prenatal mouse hippocampus tissue and these neurons were subsequently plated onto the TAT conjugated silicon nanowire device array for 32 hours during which the loaded sulforhodamine B can diffuse out of the polymer matrix at the tip of the nanowire and subsequently label the cell cytosol. The neurons and nanowire array were imaged with confocal microscopy. As the emissions of the Alexa Fluor 405 label and sulforhodamine B are different, they can be imaged with separate channels during confocal microscopy to capture clear, distinct images. The Alexa Fluor 405 labeled nanowires were excited with a 405 nm laser with an emission filter extending from 430 to 455 nm whereas the presence of sulforhodamine B was interrogated with a 559 nm laser with an emission filter extending from 575 to 675 nm. A top-down view, z-sectioned image, as well as a three-dimensional (3D) constructed image is shown in **Fig. 11**, where emission from the Alexa Fluor 405 dye appears blue and emission from the sulforhodamine B appears red.

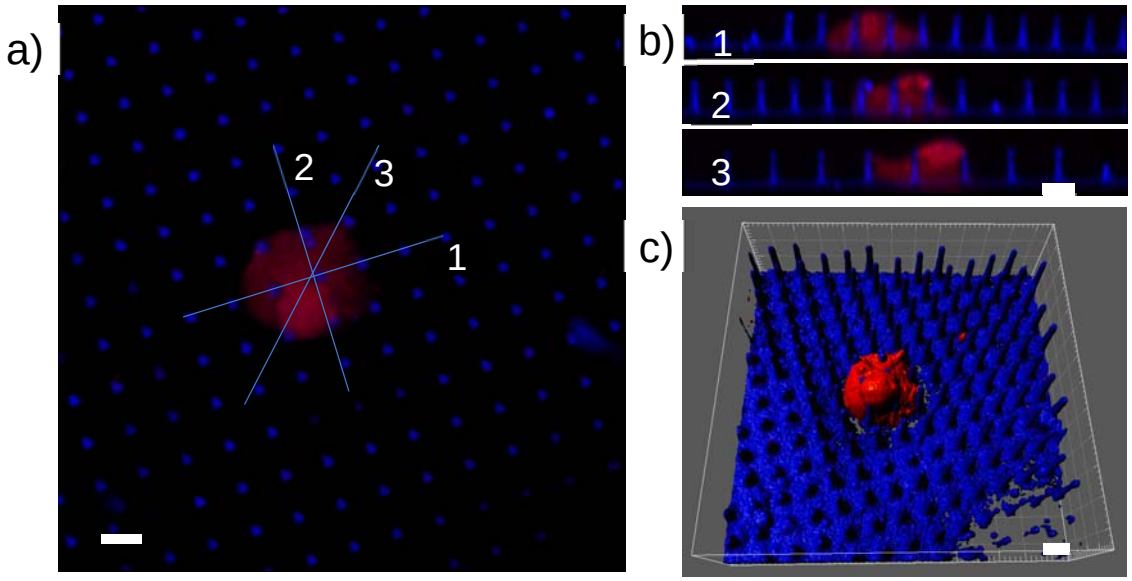

Fig. 11. Confocal microscopy images of nanowires from Figure 1 modified with TAT cell-penetrating peptides and plated with hippocampal neurons. a) Top down image. b) Z-sectioned images corresponding to the line cuts in a). c) 3D constructed image. Scale bars 5 μm.

DISTRIBUTION A: Distribution approved for public release.

As observed in the confocal microscopy images, the cell appears to be well integrated with the nanowire array, and settles between and around the silicon nanowires. In contrast to previous work utilizing freestanding nanowires, these nanowires remain attached to the silicon substrate and thus further characterization is required to identify whether the nanowire devices remain internalized within the cell or if the cell membrane has resealed around the nanowires. We have undertaken to investigate this issue by labeling the cell membrane with a separate fluorescent dye to image the membrane position after plating. Similarly, the red emission from the cellular cytosol could be due to the diffusion of sulforhodamine B dye loaded into the nanowire tips or auto-fluorescence of the cell. One possible way to address this issue is to image the cell under similar excitation and detection conditions to determine the auto-fluorescence wavelength and intensity. Furthermore, cell viability after nanowire entry can be explored, and drugs can be utilized to change the behavior of the neuron upon cellular entry.

Objective 3: ***To design, synthesize and characterize a suite of molecular device elements that can be selectively coupled to the nanowire components to build our molecular-nanoscale circuits.***

(Nocera team – Year 1) Building on our newly developed sacrificial layer and RIE tip-cleaning methodologies, we turned to selectively modifying tips of silicon nanowires. With some optimization, we developed a reproducible procedure to selectively localize electrodeposited components on and around the tips of the nanowires. This process is shown schematically in **Fig. 12a**. Briefly, a nickel sacrificial layer and a soluble polyaniline (PANI) protective coating are sequentially deposited on the nanowire. The top of the PANI protective coating is then removed physically through argon RIE etching, exposing the nickel sacrificial layer. A timed wet etch is used to remove a portion of the nickel layer (from top to bottom), resulting in only a portion of the tip of the silicon nanowire available for further modification. The desired material is then deposited on the exposed nanowire tip (Au in this case). Finally, removal of the sacrificial nickel layer and PANI protective coating through wet etching and dissolution results in the final nanowire structure as shown in **Fig. 12b,c**. We found that a PANI protective coating is necessary to direct electrodeposition to the tips of the nanowires. Without the protective coating, electrodeposition preferentially occurs on the conductive nickel shell, resulting in an unselective deposition. This method is effective for preparing tip-modified silicon nanowires with high fidelity.

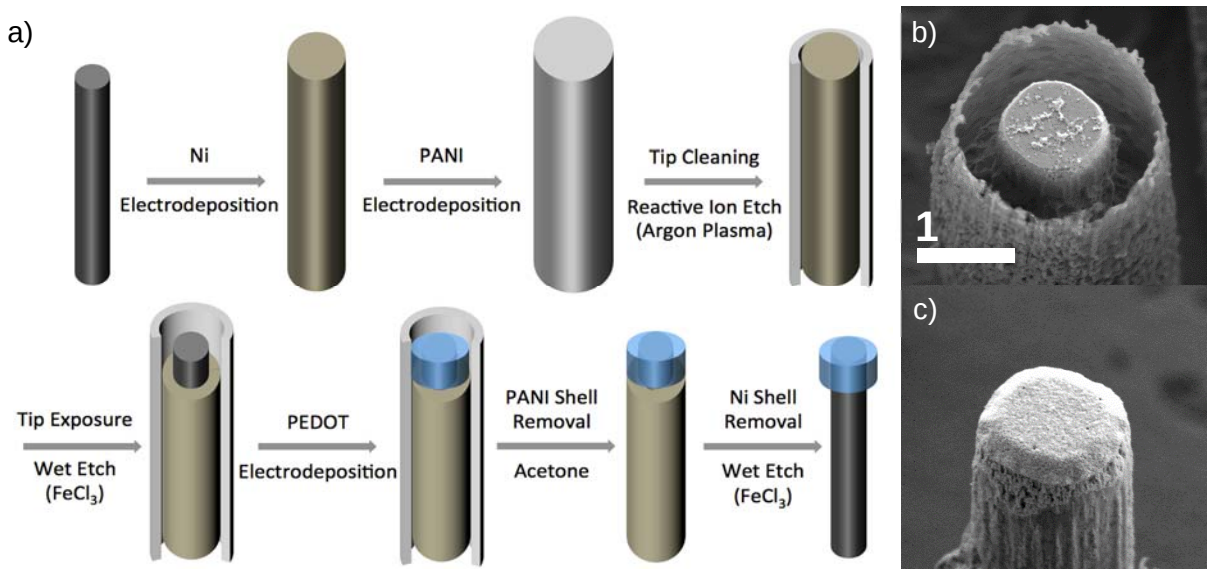

Fig. 12. a) Scheme showing procedure for tip selective electrodeposition on silicon nanowires. b) Exposed silicon nanowire after timed wet etch of Ni sacrificial layer. c) Representative nanowire with selective tip deposition (Au).

With protocols established for localized deposition on silicon nanowire tips, we turned our attention to developing tip-coupled nanowire devices. Electrochemically activated PEDOT has been investigated owing to its use for small molecule/drug delivery.[26] Films of PEDOT may be electrodeposited in the presence of drugs or other small molecules, which causes these molecules to be loaded into the PEDOT film via electrostatic and/or other intermolecular forces. Electrochemical activation by cyclic voltammetry results in conformational and electrostatic changes within the PEDOT layer, releasing the loaded molecules. We have demonstrated that this technique can be transferred to our nanowire system. Using the procedure shown in **Fig. 12a**, PEDOT was selectively deposited at the tips of the nanowires in the presence of a fluorescent dye, sulforhodamine B. The resulting nanowires are shown in **Fig. 13a**. Wires were removed from substrate by sonication. Confocal microscopic imaging of these isolated nanowires confirms the presence of sulforhodamine B localized at the tips of the nanowires (**Fig. 13b**). This result presages our ability to modifying the tips of nanowire devices to control cellular behavior. We have begun experiments to quantify the stimulated release of dyes or drugs from these tip-functionalized nanowires. We are also exploring the cellular entry mechanisms of these novel nanostructures.

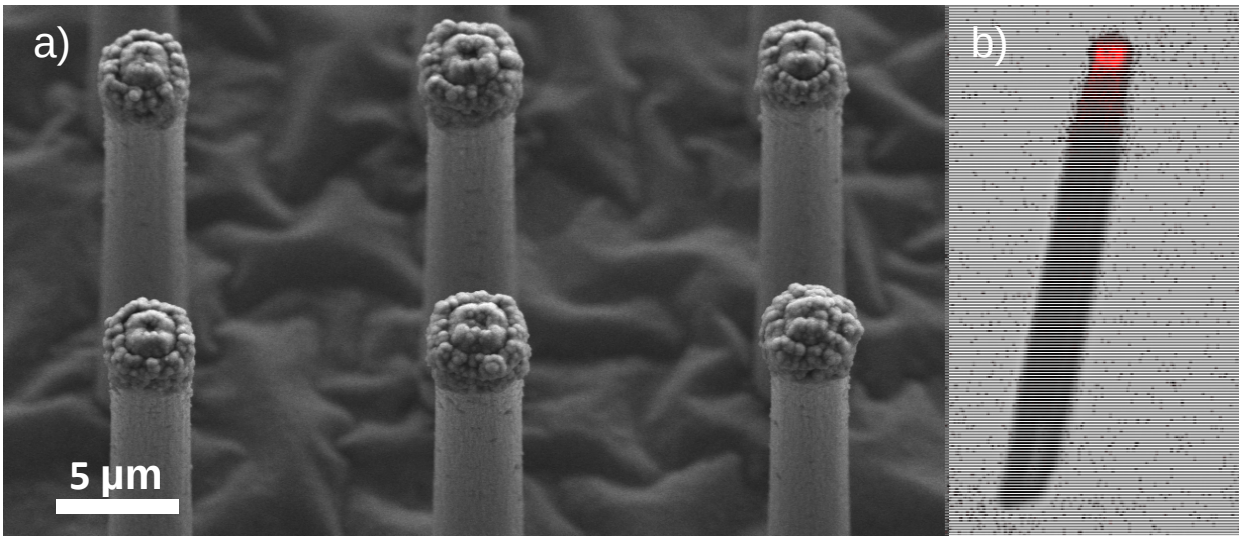

Fig. 13. a) Electron microscope image of silicon nanowires with Sulforhodamine B loaded PEDOT deposited at the tips. b) Corresponding confocal microscopy image of sonicated wires demonstrating fluorescence localized at the PEDOT tips of the nanowires.

(Lieber team – Year 2) In the first year of this project we designed and fabricated a silicon nanowire (Si NW) based electronic device to create a three-dimensional (3D) free-standing probe.[19] A kinked Si NW forms the tip of the probe, which features an integrated p-type/n-type (p/n) or p-type/intrinsic/n-type (p/i/n) junction and nanoscale p-n diode localized at the depletion region of the junction (**Fig. 14a,b**). Our group has previously demonstrated this nanoscale p-n nanowire as a field-effect transistor (FET) for intracellular electrical recording in forward bias.[1,27] In the second year of this project, we utilized the nanoscale p/i/n junction in reverse bias to demonstrate that the junction can create a localized electric field sufficient to open voltage-gated ion channels in primary neuron cells and consequently stimulate neuronal activity with several key advances made as described below.

Characterization of p/i/n junction-encoded Si NW device. For the characterization of p/i/n Si NW, a test device was fabricated using electron-beam (e-beam) lithography. Electronic properties were tested in the recording solution (Tyrode's solution). Current versus voltage (I−V) data show no measurable current in reverse bias and an onset for current flow at 0.6 V in forward bias (**Fig. 14c**).

Representative conductance versus water-gate voltage (V_g) data demonstrate a p-type FET response with sensitivity of 225 nS/V. The average reverse bias breakdown voltage in the recording solution is

approximately -2.2 V, although this number can be as high as -4 V in some nanowires. The leakage currents after reverse bias breakdown and metal contact are as small as 0.9 nA and 1.8 nA, respectively (**Fig. 14d**). It has previously been reported that current injection into the cell can induce abrupt changes in membrane potential and a burst of action potential firing, especially for neurons.[5] However, the minimum threshold of this current injection is *ca.* 470 nA, which is orders of magnitude higher than the current leakage from the nanowire device, and its effect is minimal (**Fig. 14e**).

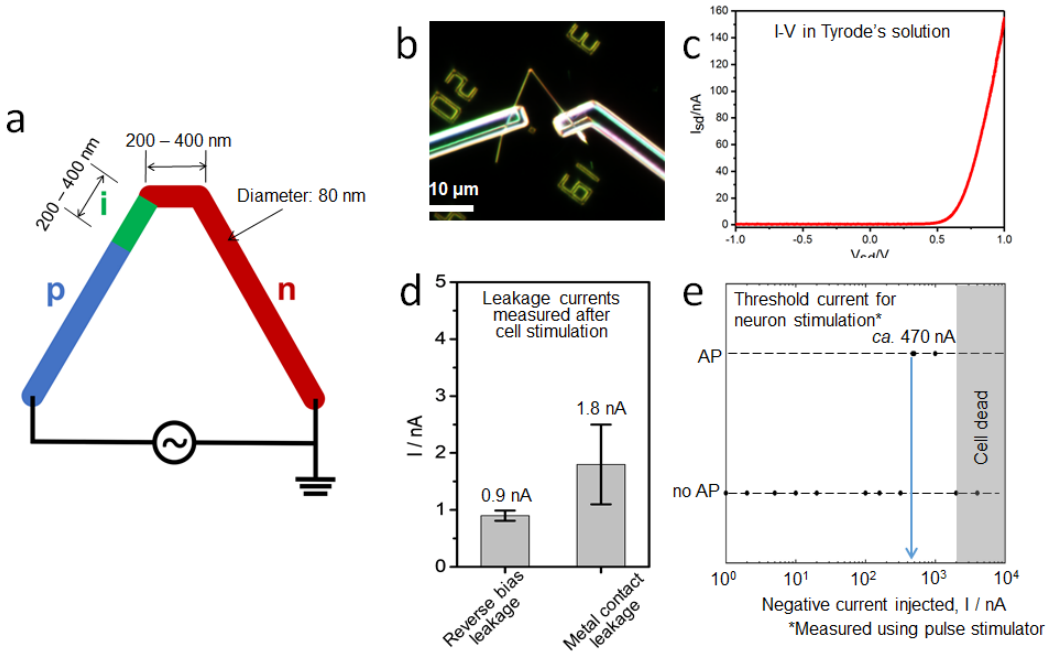

Fig. 14. Design and characterization of p/i/n kinked nanowire. a. Schematic of a kinked p/i/n nanowire with 60° kinked angle. Blue, green, and red color represent p-doped, intrinsic, and n-doped silicon segments, respectively. b. Dark-field microscope image of the kinked p/i/n nanowire nanoelectronic device. **c.** Current vs. voltage plot from device in (b). d. Current leakage averaged over multiple p/i/n nanowire devices. Current leakage in reverse bias is measured at -2.2 V. e. Threshold current for neuron stimulation, measured from cell-attached patch pipette using pulse generator. Action potential (AP) appears at ca. 470 nA injection. Cells die at >1000 nA injection.

Neuronal actuation with p/i/n NW device. The resulting free-standing p/i/n NW probes were used to target and stimulate the neuron, for example, a dorsal root ganglion (DRG) cell. The glass patch pipette was used to record the membrane potential of the neuron in the whole-cell current-clamp mode with no injected current, then the NW probe was brought into contact with the cell membrane to form an inward 'dimple' (**Fig. 15a**). Bright field microscopy shows the patch pipette and NW probe targeting the same DRG neuron (Fig. 15b). In this configuration, reverse bias voltage at -2 V with 500 ms duration was applied to the p/i/n NW device to generate an electric field and actuate ion channels on the membrane in touch with the NW (**Fig. 15e**). The voltage applied to the NW was slowly ramped from 0 to -2 V to avoid capacitive current generation. Membrane potential was continuously recorded by patch-pipette during stimulation of the cell with the NW probe (**Fig. 15c**). The results show that the firing of action potential is observed when the voltage applied to the NW reaches -2V, or at the beginning of the stimulation window. The membrane potential before and after stimulation remains stable, confirming that the stimulation procedure does not harm the cell membrane. Additionally, NW current recorded during forward bias applied to NW probe before and after the stimulation window shows that the device is consistent and

reliable (**Fig. 15d**). The NW current recorded during forward bias does not show any coupling effect with the cell membrane, demonstrating that the device is well passivated electrically, with no current leaks.

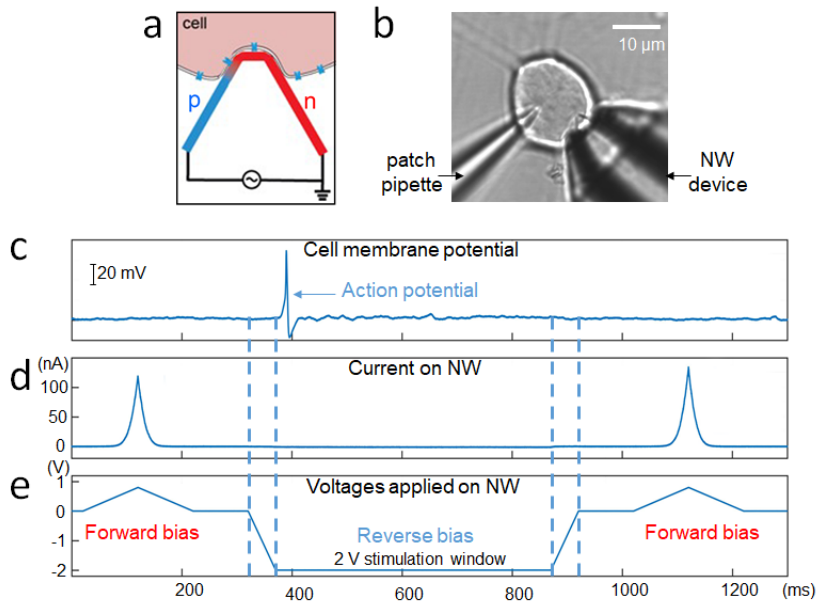

Fig. 15. Neuron stimulation with p/i/n NW device. **a.** Schematic of experimental set-up. **b.** Microscope image of patch pipette and NW device mounted on DRG cell. **c.** Action potential recorded from the patch pipette. **d.** Current recorded from NW device. The p/i/n property is characterized from the measured current at forward and reverse bias regions. **e.** Voltages applied to p-arm of NW, while n-arm is grounded. -2 V of reverse bias is applied as a stimulation window.

In some cases, DRG cells exhibit repetitive firing of action potential when stimulated with the NW probe (**Fig. 16**). The kinds of sodium channels expressed on the membrane of a DRG cell, and their distribution, vary from cell to cell. It is known that DRG cells with higher density of $Na_V1.8$ channels tend to recover

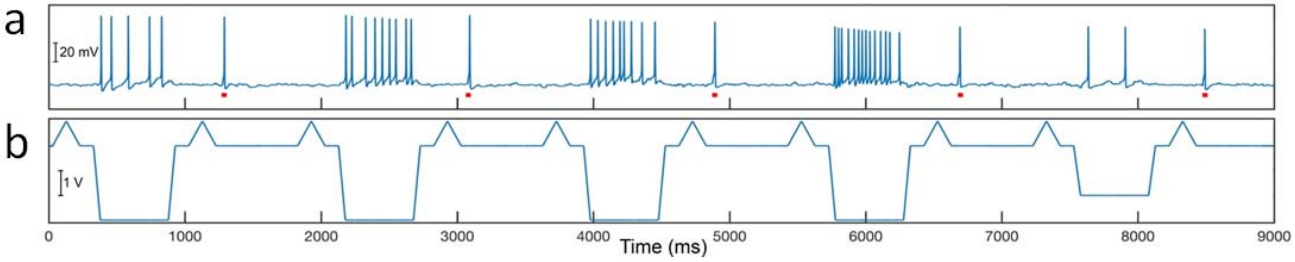

Fig. 16. Continuous firing of action potential as train of pulses for 9 secs of recording. **a.** Cell membrane potential recorded from the same DRG cell. **b.** Voltage applied to p-arm of NW. Reverse biases applied to NW are -3 V and -2 V. The red dots denote pipette stimulation with 30 nA of current injection.

from inactivation rapidly, allowing repetitive action potential firing.[28,29] In our case, -3 V of reverse bias applied to the NW can induce trains of action potential only at the stimulation window. Note that the firing frequency is reduced when the applied voltage of reverse bias decreases to -2 V.

Last, we used the p/i/n Si NW probe to actuate a single axon of the DRG cell (**Fig. 17**). To do this, the DRG cell is cultured in the incubator for over 24 hours to allow axons to grow out from the soma. Once the axons are visible under a microscope, the NW probe is brought into contact with the axonal initial segment (AIS) while the glass patch-pipette is recording the intracellular membrane potential of the cell in a whole-cell patch clamp mode. Reverse bias of -2 to -3 V is applied to the nanowire, successfully inducing firing of action potentials recorded at the soma of cell. The action potential only appears when the NW probe is in touch with the cell membrane, and disappears when the probe is removed.

DISTRIBUTION A: Distribution approved for public release.

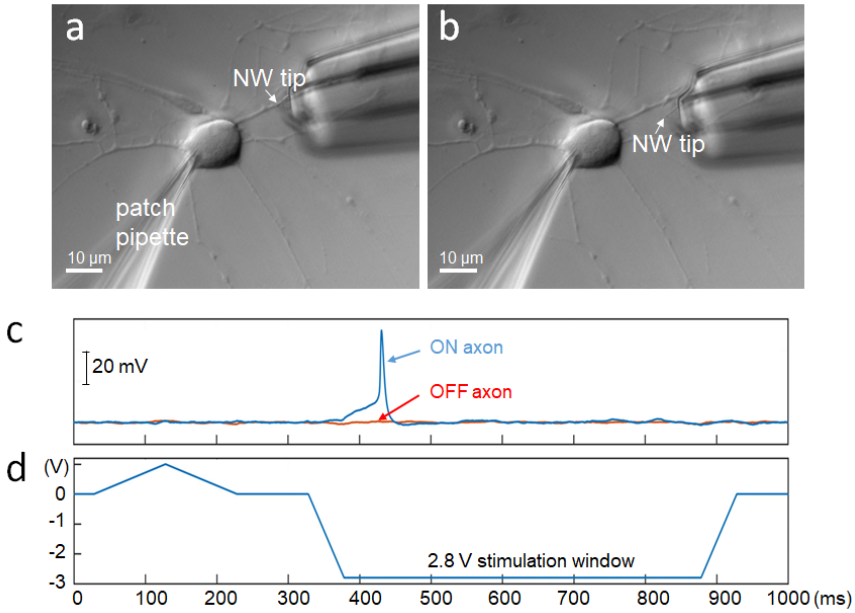

Fig. 17. Axonal stimulation of DRG cell using p/i/n NW probe. a, b. Microscope image taken during the recording where NW is touching the axonal initial segment (AIS) (a) and away from the cell (b). c. Action potential recorded from the patch pipette on the soma of cell. d. Voltages applied to NW for stimulation.

Electrochemical modification of nanowire tips. (Nocera team – Year 2). The methodology to prepare tip-modified nanowire architectures, although reliable, is time and energy consuming due to multiple synthetic steps. Furthermore, it may lead to introduction of toxic contaminants such as residual nickel (a sacrificial segment of the methodology). As such, we developed a new, reproducible method to prepare selective deposition on nanowires. Two pathways for this technique were developed and are shown in **Fig. 18**.

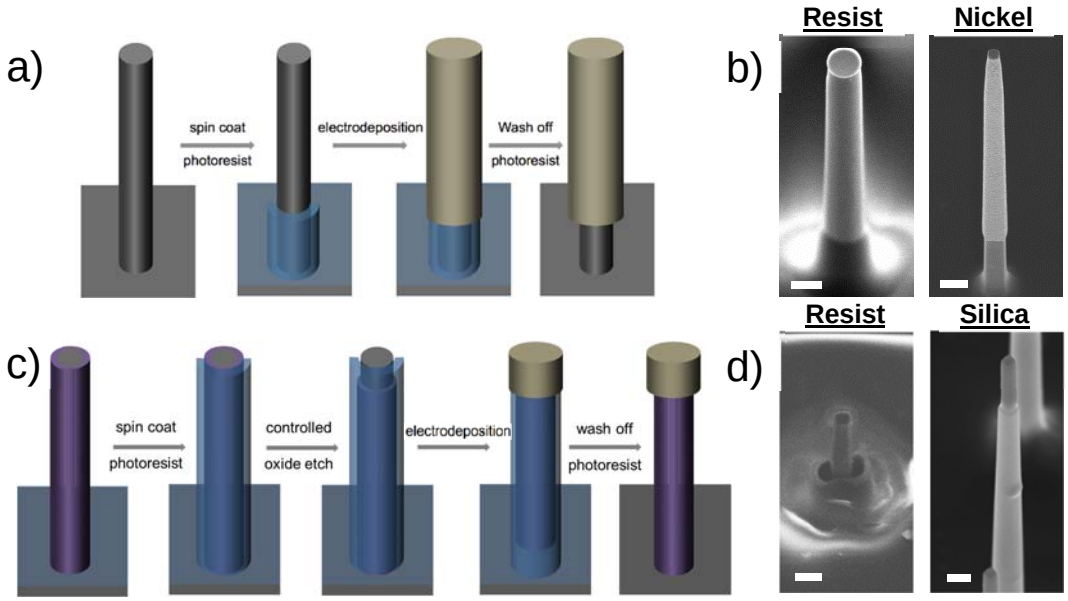

Fig. 18. a) Scheme showing procedure for substrate masked electrodeposition on silicon nanowires. b) Exposed silicon nanowire after spinning of photoresist (left) and nickel coated nanowire after removal of photoresist (right). c) Scheme showing procedure for tip selective electrodeposition on oxide coated silicon nanowires. d) Exposed silicon nanowire tip after spinning of photoresist and timed etch with buffered oxide etch with (left) and without (right) photoresist mask layer. Scale bars 1 µm.

In **Fig. 18a**, a photoresist layer is spincoated onto a silicon nanowire array to serve as a mask during electrodeposition. The photoresist layer covers the silicon substrate as well as a portion of the bottom of the silicon nanowires; electrodeposition thus only occurs on the exposed silicon (conductive) portion of the nanowires. Removal of the photoresist in acetone yields selectively modified nanowire arrays (**Fig. 18b**). With this technique, only the bottom portion of the wires are protected by photoresist while exposing a large portion of the wire body, making tip-selective functionalization difficult. As shown in **Fig. 18c**, we addressed this challenge by utilizing a change in the wetting behavior of photoresist by thermally converting the outer layer of the wires to silicon oxide in a wet-oxide furnace. Spincoated photoresist now wets up to the top of the nanowire arrays and a time controlled etch of the oxide layer from the top side of the wire using a buffered oxide wet chemical etchant now only exposes the top portion of the nanowires (**Fig. 18d**). Electrodeposition will only occur on the exposed bare silicon tip of the nanowire where both the oxide layer and photoresist act as a mask toward electrodeposition. Finally, removal of photoresist and the remaining oxide yield tip-modified silicon nanowires (**Fig. 10**). We found that the photoresist is necessary to permit directional etching of the oxide layer only at the exposed silicon nanowire tips.

We also investigated other architectural components that can be integrated into nanowire devices. Mesoporous silica has been widely explored in the literature as a method for stimuli molecular release.[30-32] Once loaded with active molecules, the pores can be capped and triggered to release cargo upon stimulation with light and various chemical stimuli such as pH and small molecules.[31,32] Mesoporous silica is typically synthesized as nanospheres and thus can be limited in inherent functionality as well as ability to introduce novel functionality. A previous report demonstrates that the growth of mesoporous silica on flat metallic substrates can be directed electrochemically from a colloidal solution containing tetraethyl orthosilicate as a silicon source and cetrimonium bromide as a templating agent. Following calcination at 130 ^{o}C, the template can be removed with dilute hydrochloric acid.[33] We have demonstrated that this technique, with some optimization, can be adapted to our nanowire platform to allow electrodeposition of conformal layers of mesoporous silica around both functionalized and bare silicon nanowires. Mesoporous silica layers can be grown on metal (such as gold) and bare silicon nanowires by applying -1200 mV and -1600 mV vs. a Ag/AgCl reference electrode, respectively, where the thickness of the mesoporous shell is controlled by deposition time. Scanning electron microscope images of nanowires modified with mesoporous silica are presented in **Fig. 19**.

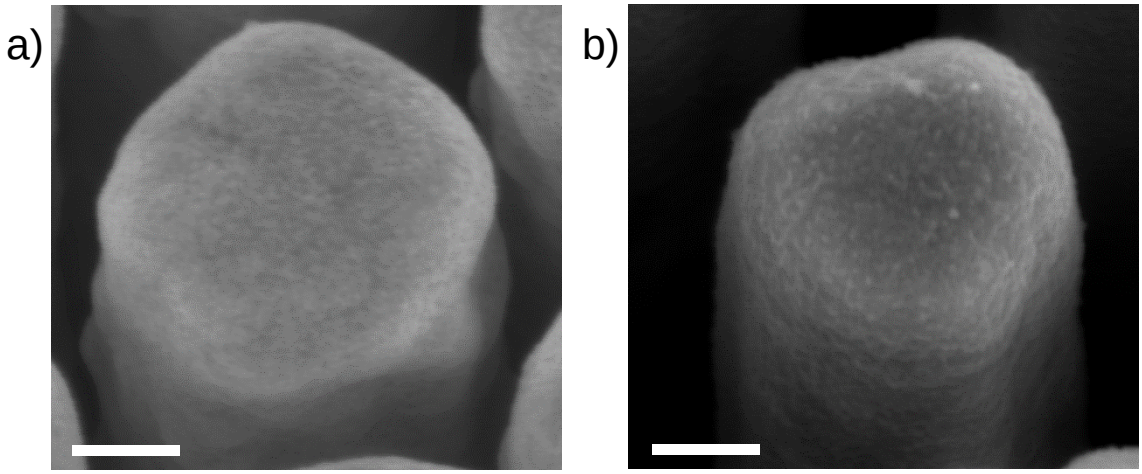

Fig. 19. Mesoporous silica films deposited on a) gold coated silicon nanowires and b) bare silicon nanowires. Scale bars 200 nm.

As metal-coated nanowires can be functionalized with mesoporous silica at a lower potential than bare silicon, we are able to selectively modify certain components of nanowire devices. In conjunction with our tip-selective deposition methodology, we believe that a wide variety of potential device architectures

DISTRIBUTION A: Distribution approved for public release.

are accessible, such as a single nanowire device that can release different small molecules depending on the applied stimulus.

(Nocera team – Year 3) In our previous report, we detailed the synthesis of silicon nanoprobes with sulforhodamine B, a fluorescent dye, loaded into polypyrrole-functionalized nanowire tips. Following our investigations on the cellular entry mechanisms of this prototypical device design we focused on exploring the encapsulation properties of the polymer medium that regulates the diffusion rate of the dye released. We determined that sulforhodamine B spontaneously leaks from polypyrrole when prepared by the oxidation of the monomer in an aqueous solution of 0.1 M $LiClO_4$. The diffusion was attributed to high film porosity resulting from side reactions with water during polymerization. Water may act as a nucleophile to terminate growing polypyrrole chains or to disjoint chain aromaticity,[34] as shown in reactions 1 and 2.

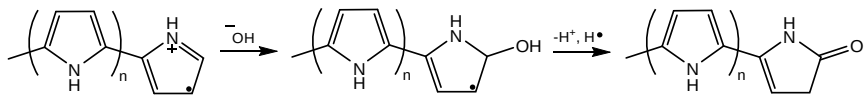

(1)

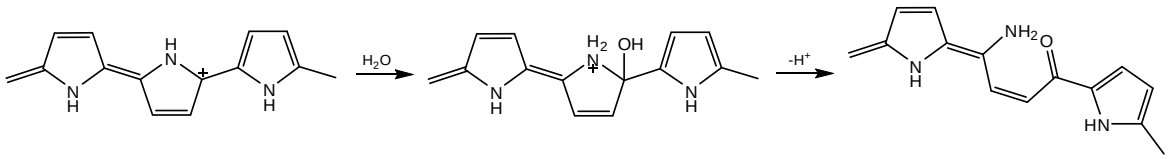

(2)

As an alternative oxidation medium, we modified our deposition protocol to run the electrochemical oxidation reaction in acetonitrile (50 µL pyrrole in 3 mL of 0.01 M $LiClO_4$ dissolved in acetonitrile under cyclic deposition between 0.5-1.5 V *vs.* Ag/AgCl reference electrode at 50 mV/s scan rate for 5 cycles). As a result, polymer porosity was minimized and film integrity maximized (**Fig. 20**). We observed that polypyrrole films deposited from acetonitrile showed improved adhesion as well as the ability to maintain sulforhodamine encapsulation for more than 72 hours, giving enough time for the incubation of cells on nanoprobes (6-32 hours).[19] While slight dye diffusion is observed over the 72-hour period, wires labeled with rhodamine clearly continued to fluoresce stronger than those with neither dye nor polymer.

When polypyrrole films containing sulforhodamine B were incubated in water for 72 hours, the water fluoresces with a similar profile to sulforhodamine B (Fig. 18a), demonstrating dye leakage from the polymer. To improve film quality, the electrolyte solvent was changed from water to acetonitrile and the deposition process was changed to include a capping stage. The change of solvent prevents side reactions 1 and 2, while the capping with pyrrole provides an extra layer of film separating dye from liquid media.

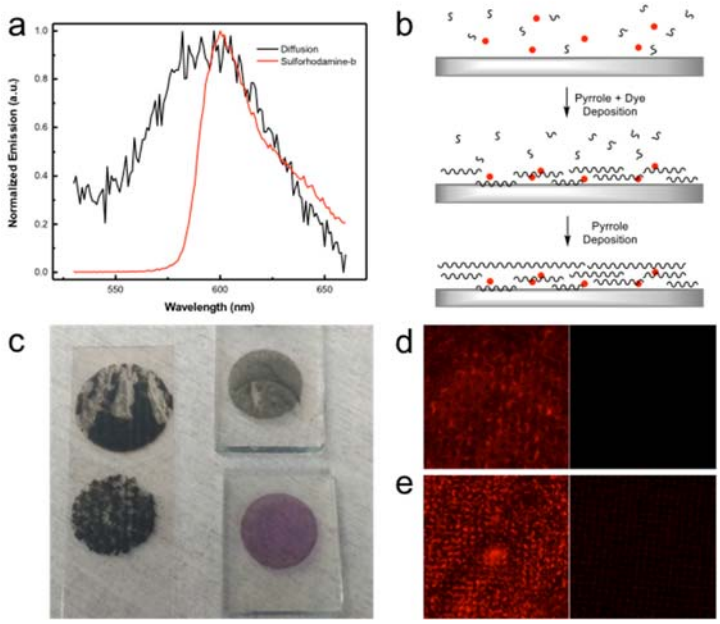

Fig. 20. a) Normalized fluorescence of aqueous diffusion layer compared to aqueous sulforhodamine B. b) Schematic illustration of modified pyrrole electrodeposition from acetonitrile. Pyrrole and dye are first deposited in tandem, then the film is capped with a thin layer of polypyrrole to minimize leaking. c) Visual comparison of water-deposited polypyrrole (top left), water-deposited polypyrrole and sulforhodamine B (bottom left) acetonitrile-deposited polypyrrole (top right), and acetonitrile-deposited polypyrrole and sulforhodamine B (bottom right). d) Confocal microscopy image of dye-loaded polypyrrole on nanowire arrays (left) and unlabeled arrays (right). e) Dye-loaded polypyrrole on nanowire arrays (left) and unlabeled arrays (right) after 72 hours in water.

DISTRIBUTION A: Distribution approved for public release.

These two changes to the electrodeposition conditions yielded films with greater adhesion as well as visible color change upon the addition of dye (**Fig. 20c**). While polypyrrole deposited from acetonitrile onto wires showed some dye diffusion over the course of 72 hours, the signal-to-noise ratio remained high enough to easily distinguish between areas labeled with dye and those without dye (**Fig. 20d,e**).

Objective 4*: To selectively couple specific classes of molecular devices to nanowire antenna elements required for transport of photons or charges.*

(Nocera – Year 3) Extending the capabilities of our tip modified nanoprobes, we developed a new protocol for the deposition of colloidal quantum dots on silicon nanoprobes. Our protocol is based on a layer-by-layer deposition approach;[35,36] the electrostatic interactions between a negatively charged substrate and oppositely charged polyelectrolyte monolayers allows for the layer-by-layer deposition of thin polymer layers and also the attachment of charged nanoparticles on flat surfaces. For our 1D nanoprobe studies, we first optimized the deposition conditions on large wire arrays. Following the preparation of our micro/nanowire arrays, detailed in our recent publication,[25] there exists a native oxide formation on the silicon surface due to air exposure. This thin silicon dioxide layer on the wire surface is negatively charged and serves as an electrostatically attractive interface for a positively charged polyelectrolyte. We used PEI: poly(ethyleneimine) as the positive electrolyte (polycation) and PSS: poly(sodium 4-styrenesulfonate) as the negatively charged electrolyte (polyanion). Following 3 iterations of positive and 2 iterations of negatively charged polyelectrolyte layer depositions (wires were dipped into 1% polyelectrolyte in 0.1 M NaCl solutions at pH 5 and subsequently washed in deionized water to remove the excess layers which are not electrostatically bound), negatively charged CuInS/ZnS core/shell quantum dots were decorated on the wires. A simplified schematic of the procedure and advanced atomic and elemental analysis of the modified wires are shown in **Fig. 21.**

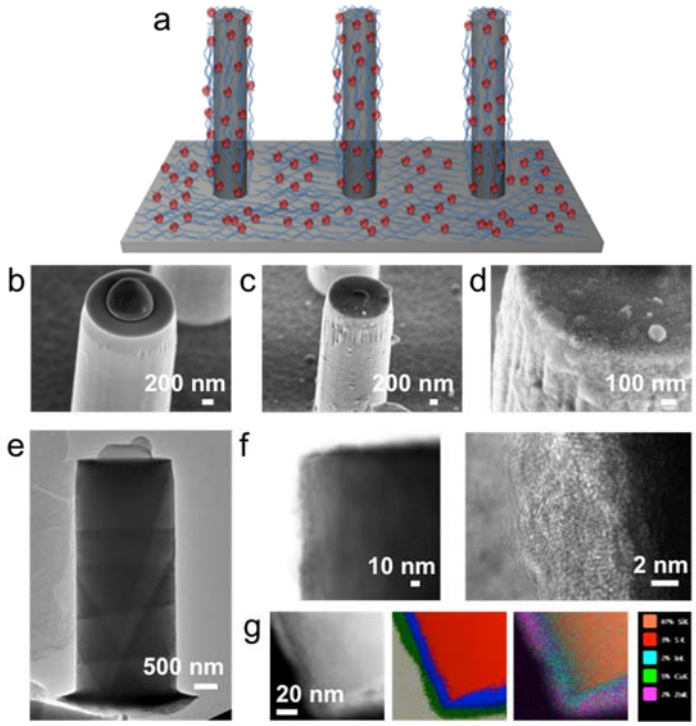

Fig. 21. a) Scheme showing procedure for deposition of polyelectrolytes (blue) and quantum dots (red) on silicon wires (gray). Scanning electron microscope images of b) a bare silicon wire, c) after layer by layer deposition of polyelectrolytes and quantum dots, d) higher magnification image of the same wire. e) Transmission electron microscope image of a silicon wire cut from the array. f) high magnification images of the corner of the wire tip

photoresist (left) and ultra-high-resolution image of the quantum dots at the wire tips (right). g) Transmission electron microscope image, phase map, and elemental map of the corner of the wire tips, respectively.

We then developed a procedure to attach quantum dots specifically at the tips of the wires by embedding the wire array in a photoresist matrix. SU-8 photoresist was spin coated at 3000 rpm and the tips of the wires were cleaned with a 1 min 100 W oxygen plasma to expose the tips of the wires (**Fig. 22a**). A similar layer-by-layer deposition approach was followed as discussed above to attach the quantum dots and the sacrificial resist was subsequently lifted off using an SU-8 developer solution (**Fig. 22b**).

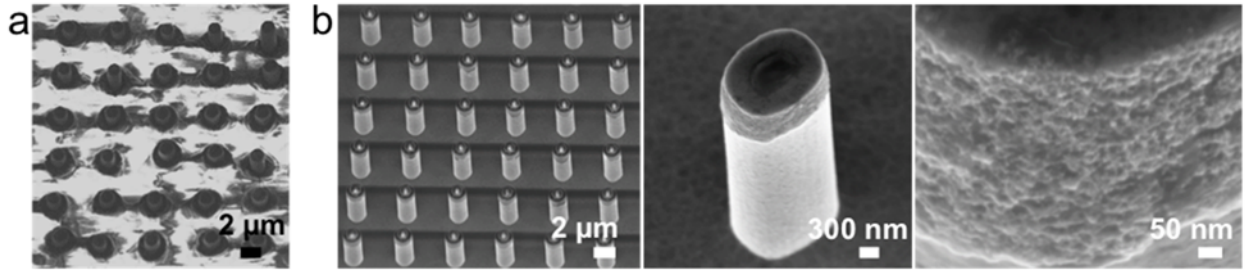

Fig. 22. a) Scanning electron microscope image of a silicon wire array after photoresist embedding and oxygen plasma steps. b) Same wire array after layer-by-layer deposition and photoresist removal, where the images are presented in higher magnifications from left to right.

After the optimization of the wire modification with layer-by-layer assembly we focused on the deposition conditions on nanowire arrays that we use in our nanoprobe studies. Two types of quantum dots were attached separately and were analyzed with electron and optical microscopy as shown in **Fig. 23**. The optical properties of the colloidal quantum dot emitters suspended in water (**Fig. 23a**) were preserved once they were assembled on nanoprobes (**Fig. 23b-d**) as confirmed by the top-view confocal microscopy image presented in **Fig. 23e**.

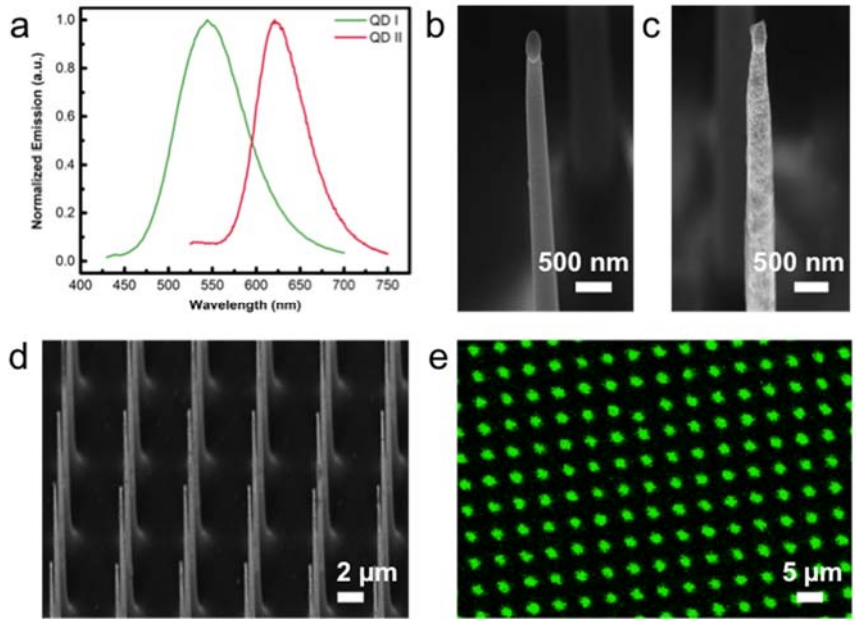

Fig. 23. a) In-solution fluorescence spectra of the quantum dots used in layer-by-layer deposition. Scanning electron microscope image of a b) bare silicon nanoprobe, c) quantum dot decorated nanoprobe. d) Scanning electron microscope image of an array of silicon nanoprobes (diameter of ~125 nm and length of 13 µm) prepared with quantum dots featuring emission peak at 545 nm. e) Confocal microscope image of the nanoprobe array taken under laser excitation at 405 nm.

Coupled with the ability to selectively modify the tips of the nanowires, the unique ability of the nanoprobes to penetrate into cellular systems while maintaining the integrity and the optical detectability of the nanoprobes makes this a great molecular nanoscale circuit platform for active control of cells.

Objective 5*: To investigate fully assembled molecular-nanoscale circuits for controlled internalization and subsequent optical control of cellular function using single cell assays.*

(Lieber team – Years 2 and 3) **Fabrication and characterization of scalable three-dimensional ultrasmall nanowire field effect transistor probes.**[37] Integration and internalization of nanoscale circuits within single cells and/or different cells requires development of scalable circuit elements that are on the same length scale as that of biologically relevant subcellular structures. To attain this goal, we synthesized molecular-nanoscale p-type Si nanowires (p-Si NW) with 15 nm diameters using gold nanoparticle-catalyzed chemical vapor deposition and combine deterministic shape-controlled nanowire transfer with spatially-defined transformation of silicon to nickel silicide to realize U-shaped nanowire

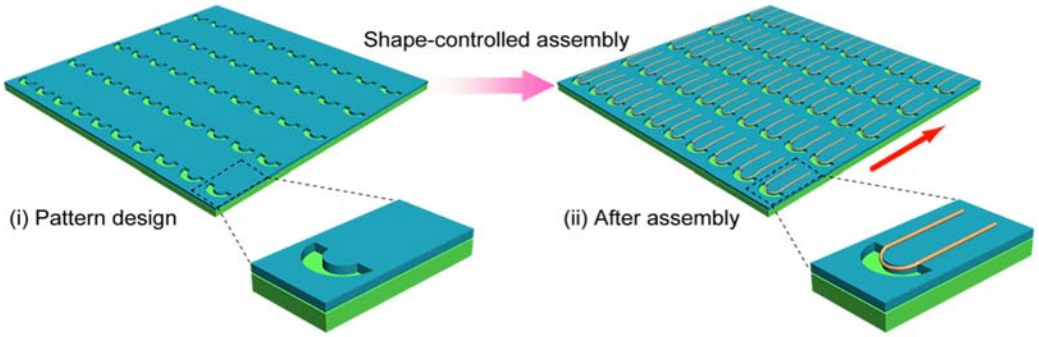

Fig. 24. Schematic showing large-scale, shape-controlled deterministic nanowire assembly.

field effect transistor (U-NWFET) arrays with controlled radii of curvature and localized sensing channel at the U-shaped nanowire tip.

Specifically, we use large-scale, shape-controlled deterministic nanowire assembly (**Fig. 24**)[38], to realize arrays of U-NWs with controllable radius of curvature (ROC) assembled on the top of predefined regions of bottom Si_3N_4 passivation layers and Ni sacrificial layers at each specific probe position. The transferred U-NWs are electrically addressed via deposition of Au/Cr metal interconnects which are then covered by an upper Si_3N_4 passivation layer. Then, we exploit spatially-defined solid-state transformation to convert Si NW segments underneath and adjacent to Ni diffusion layer to metallic NiSi (**Fig. 25a, b**). As the NiSi portion of the NW has substantially higher conductance than p-silicon,[39] the conductance of the circuit will be dominated by the remaining p-Si at the tip of the NW, thereby producing a controllable length of Si FET sensing elements at the tip of the U-NW probes. Composition-sensitive SEM images of U-NWFET (**Fig. 25c**) highlight the designed channel lengths of ca. 50 nm, 0.5 μm and 2 μm respectively. Removal of the sacrificial layer allows the devices to bend upward due to interfacial strain in the metal interconnects, yielding single U-NWFET probes (**Fig. 25d**) or probes with up to four U-NWFETs per bend-up probe arm (**Fig. 25e**). The electrical transport properties of U-NWFET probe arrays with different channel lengths of ca. 50 nm, ca. 0.5 μm, ca. 2 μm are characterized, yielding average conductances of 3.3 ± 0.6, 0.7 ± 0.2 and 0.3 ± 0.1 μS and average sensitivities of 0.56 ± 0.12, 0.26 ± 0.07 and 0.07± 0.03 μS/V, respectively (**Fig. 25f-h**). The noise level of the devices is in the range of 0.5-1.5 mV for probes with different channel lengths, which should allow detection of subthreshold activities of electrogenic cells, which are on the order of 1-10 mV.

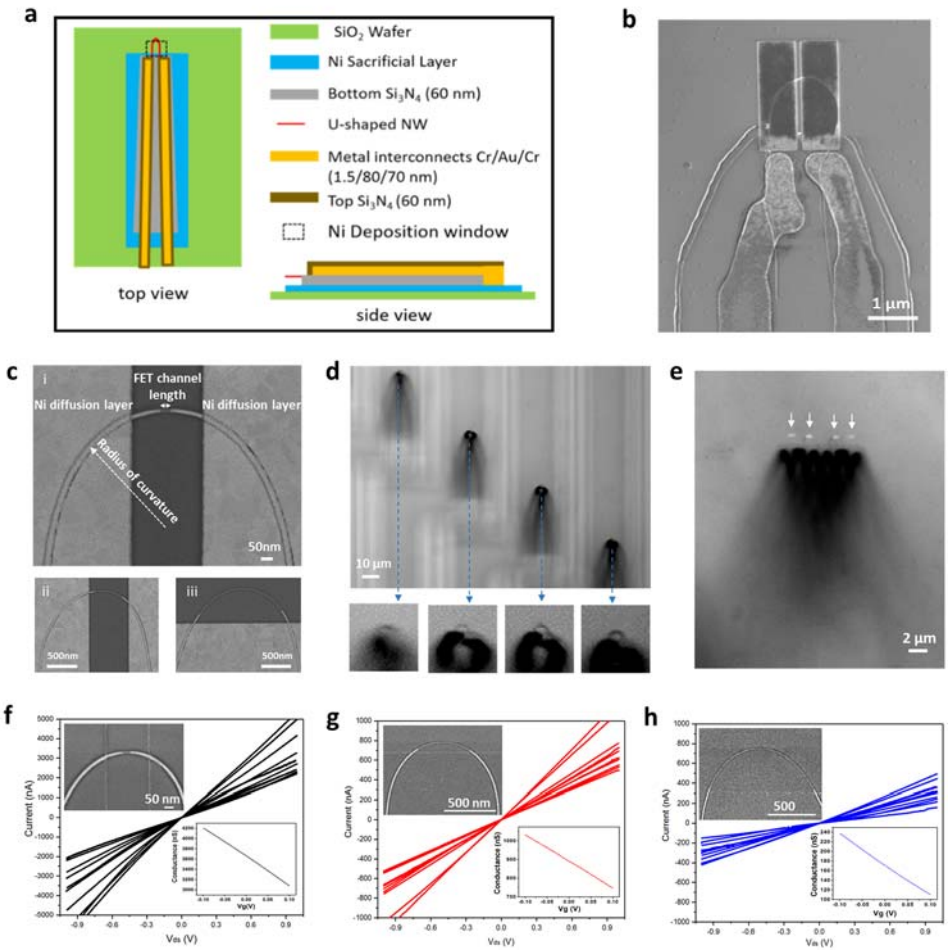

Fig. 25. Fabrication and characterization of U-NWFET probes. a, Schematics of device fabrication. **b**, SEM image of device after Ni diffusion. **c**, Zoom-in SEM image of device after Ni diffusion with different FET channel lengths: (**i**) ca. 50 nm, (**ii**) ca. 0.5 µm (**iii**) ca. 2.0 µm. Imaging with backscattered electrons (BSE) shows the Si (dark region) and NiSi (bright region) distribution on the U-NW. **d**, Optical image of array of single U-NWFET probes per bend-up arm. **e**, Optical image of 4 U-NWFETs probes per bend-up arm. **f-h**, SEM images (BSE), current versus drain-source voltage (V_{ds}), and conductance versus water-gate voltage (V_g) of probes with different FET channel lengths: (**f**) ca. 50 nm, (**g**) ca. 0.5 µm (**h**) ca. 2.0 µm.

Intracellular (IC) recording using U-NWFET probes.[37] The fabricated U-NWFET probe arrays can be functionalized with phospholipid[2] and interfaced with electrically active cells to record changes in intracellular potential during biological processes. The NWFET acts as a voltage sensor because its conductance changes as the device is gated by the varying potential of the local solution. A schematic illustrating the cell/device interface is shown in **Fig. 26**.

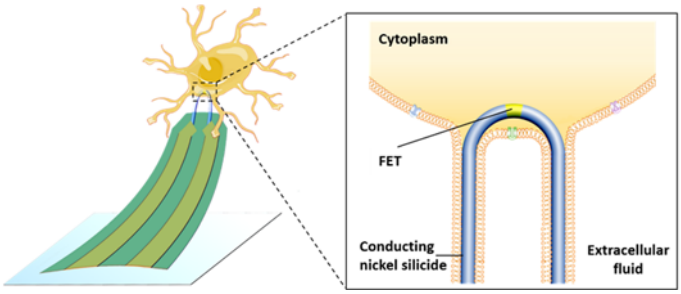

Fig. 26 Schematics of IC recording by a U-NWFET probe. The sensitive p-type Si NWFET region and the metallic NiSi region on U-NW are marked with yellow and silver respectively.

The U-NWFET probes were modified with phospholipid vesicles in a manner similar to previous work[2], and then brought into contact with the cultured dorsal root ganglion (DRG) neurons (**Fig. 26**). A single U-NWFET probe with ca. 50nm FET length and 0.75µm ROC was used to sequentially measure six spontaneously firing DRG neurons with maximum action potential signal amplitude of ca. 100 mV and noise level of ca. 0.7 mV within 1 hour without cleaning or re-modification (**Fig. 27**). These waveforms, amplitudes, firing patterns and signal-to-noise ratio of action potentials indicate that the ultrasmall U-NWFET with biomimetic phospholipid modification can obtain a high resistance seal with the membrane while achieving direct contact with the interior of the neurons. Subthreshold activities (highlighted by blue triangles in inset i, ii, iii of **Fig. 27d**) were recorded, which suggests that these devices can be used for measurement of neurons networks containing presynaptic cells and inhibitory or excitatory subthreshold activity of post-synaptic cells.

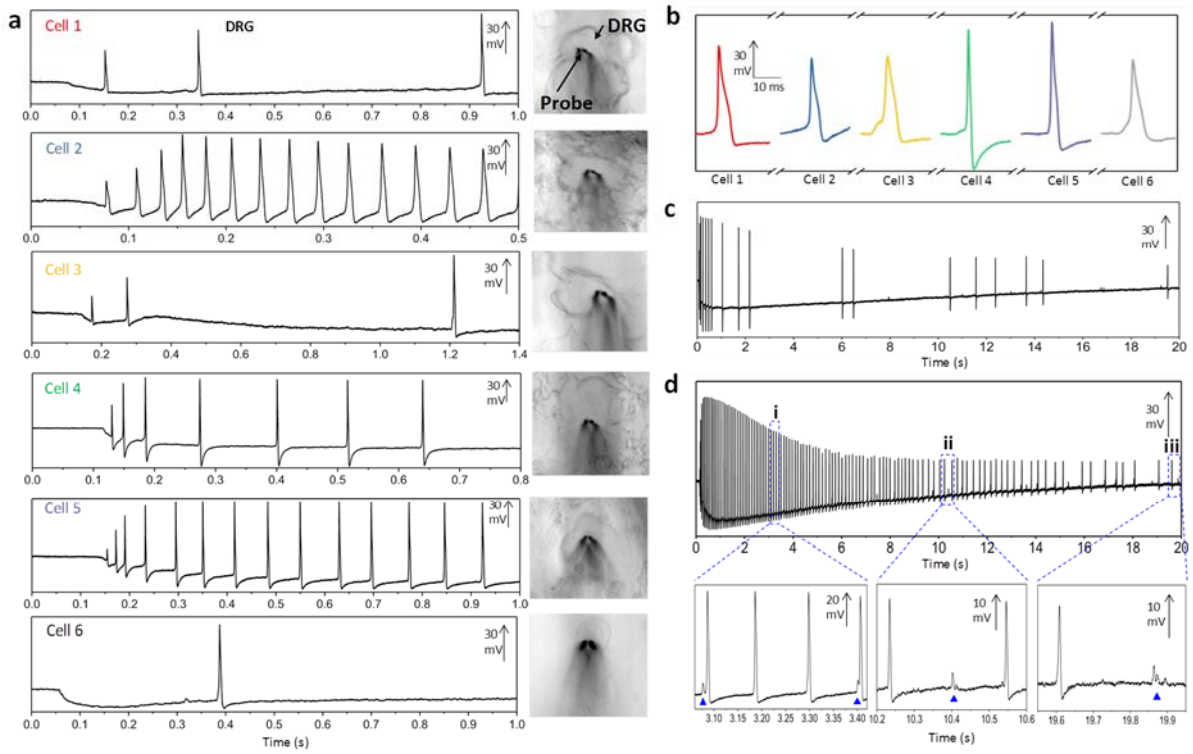

Fig. 27. IC recording of DRG neuron by ultrasmall U-NWFET probe. a, Repeatable IC action potentials recorded from 6 different neurons using the same U-NWFET probe. The numbering of the cells indicates the order in which the measurements occurred. All signals are recorded by ca. 50 nm FET probe with 0.75 µm ROC. Inset from cell 1 shows optical image of single probe recording one DRG neuron. Left show the images of DRG and probe during measurement. **b**, The summary of recorded action potentials from the 6 different cells in chronological order. Maximum signal amplitude remains similar between these measurements, showing that the probe is highly reusable. **c**, IC recording of action potential from intermittently firing neuron by U-NWFET probe. **d**, IC recording of action potential from regularly firing neuron by U-NWFET probe. Inset **i**, **ii**, **iii** are the zoom-in of action potential at ~3.1 s, ~10.2 s and ~19.5 s respectively. High amplitude and signal/noise recordings including action potential and subthreshold potentials can be observed clearly. Over time, the amplitude decays to ~20% of its maximum value, but it remains ~20 mV. Blue triangles highlight the subthreshold potentials.

To verify that our U-NWFETs can interface with a variety of different electrically active cell types, human induced pluripotent stem-cell-derived cardiomyocytes (HiPSC-CMs) were cultured and measured twice with the same probe, and action potential amplitude (ca. 50 mV) (**Fig. 28**). Notably, the action

potential frequency during the first (1.25 + 0.04 Hz) and second entry (1.23 + 0.02 Hz) as well as the action potential waveform remains the same (**Fig. 28b,c**), suggesting that U-NWFET probe internalization is minimally invasive to the cells.

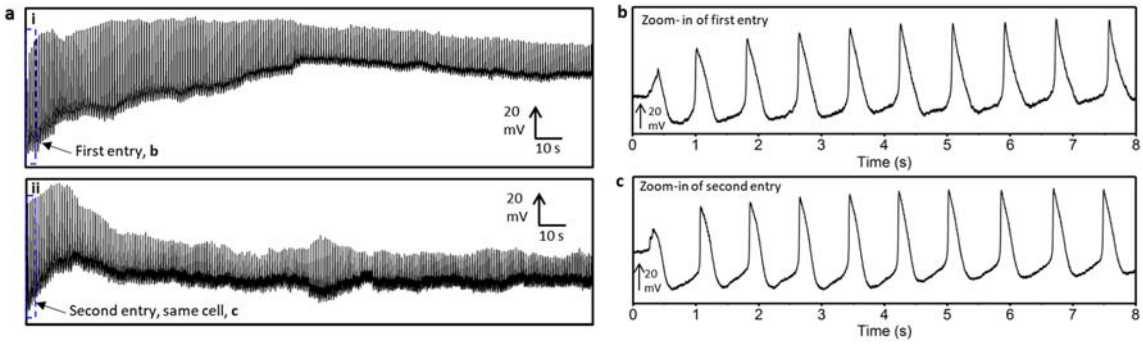

Fig. 28. Repeated IC recording from one HiPSC-CM by one U-NWFET probe with 50 nm channel length and 0.75 µm ROC. a, Two traces obtained sequentially using the same U-NWFET on the same cell. Following the (**i**) initial recording of ca. 3 mins, the probe was retracted for ca. 3 mins and (**ii**) then brought back into contact with the same cell to achieve intracellular recording again. **b**, Zoom-in traces of the initial entry and **c**, the second entry. The action potential frequencies of the HiPSC-CM between the first entry (1.25 $\pm$ 0.04 Hz) and second entry (1.23 $\pm$ 0.02 Hz) are comparable and suggest that U-NWFET probe penetration does not affect cell viability and is minimally invasive.

Geometrical control of device internalization/recording.[37] Having shown that the ultrasmall U-NWFET probes enable true IC action potential recording, we conducted a series of tests to investigate how size and geometry of the probes influence the cell/probe interface and recorded action potential amplitudes. First, we investigated how geometry affects recording by fabricating probe arrays with ROC ranging from 0.75 µm to 2.0 µm with fixed ca. 50 nm sensor size (**Fig. 29a,b,c,f,i**), and attempted ca. 30 measurements for each ROC from both DRG neurons and HiPSC-CMs. The distribution of maximum recording amplitudes from both cell types indicates that decreasing ROC increases the yield of high amplitude IC recording.

Second, we studied how sensor size affects recording by varying U-NWFET channel lengths and found that decreasing channel length results in higher amplitude recordings for both DRG neurons and HiPSC-CMs (**Fig. 29d,e,g,j**). Notably, when we compared probes with both small channel length and ROC with probes with both large channel length and ROC, we observed that ultrasmall probes (ca. 50 nm channel length, 0.75 µm ROC) yielded IC recording (**Fig. 28, Fig. 29d**), while simultaneously increasing the ROC and channel length resulted in an extracellular (EC) action potential signal (**Fig. 29e**). These systematic studies suggest that pushing the spatial limits of nanoprobes improves the interface of the U-NWFET with the intracellular space and the seal with the cell membrane and is critical for developing tools that faithfully capture intracellular action potentials.

DISTRIBUTION A: Distribution approved for public release.

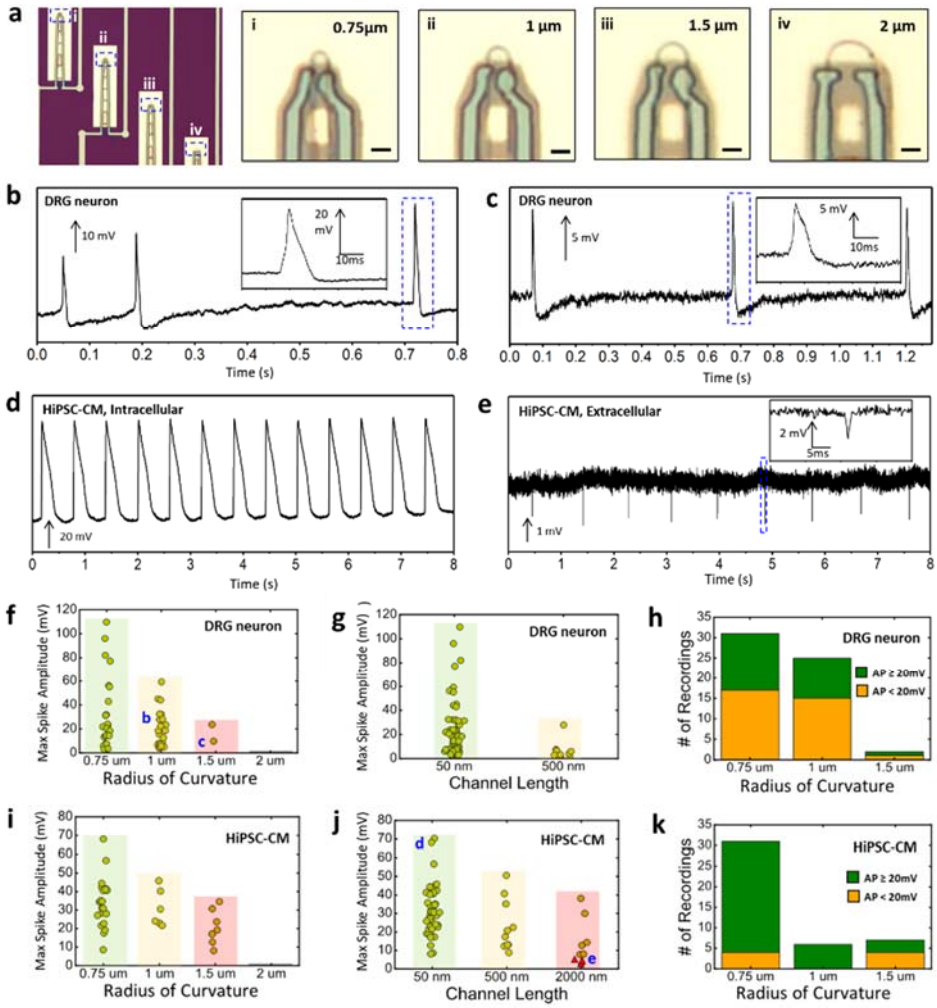

Fig. 29. Effect of size and geometry of U-NWFET probes on electrophysiological recordings from DRG neurons and HiPSC-CMs. a, Optical image of U-NWFET probes with different ROC before deposition of Ni diffusion layer (**i**) 0.75 µm, (**ii**) 1 µm, (**iii**) 1.5 µm and (**iv**) 2 µm. **b,c,** IC/IC-like recording from DRG neuron by ca. 50 nm FET channel length probe with (**b**) 1 µm and (**c**) 1.5 µm ROC. Insets are the zoom-in view of selected action potentials (highlighted by blue dashed rectangles). **d**, IC recording from HiPSC-CM by ca. 50 nm FET channel length probe with 0.75 µm ROC. **e**, EC recording from HiPSC-CM by 2.0 µm FET channel length probe with 1.5 µm ROC. Inset is the zoom-in of the selected spike. **f**, Plot of maximum recorded spike amplitude of recorded action potentials from DRG neurons versus ROC with fixed ca. 50 nm FET length. The blue letters 'b' and 'c' highlight the data points from Fig.4 b,c. **g**, Plot of maximum spike amplitude of DRG neurons versus varying FET channel lengths with assorted ROC (0.75 - 2 µm).**h**, Histogram of numbers of IC/IC-like recordings from DRG neurons vs ROC using ca. 50 nm FET length probes. The orange block indicates amplitude less than 20 mV, and the green block indicates larger than or equal to 20 mV. **i**, Plot of maximum recorded spike amplitude of recorded action potentials from HiPSC-CM versus ROC with fixed ca. 50 nm FET length. **j**, Plot of maximum spike amplitude of HiPSC-CM versus varying FET channel lengths with assorted ROC (0.75 - 2 µm). Red triangles indicate EC action potentials. The blue letters 'd' and 'e' highlight the data points from Fig.4 d,e. **k**, Histogram of numbers of IC/IC-like recordings from HiPSC-CM vs ROC using ca. 50 nm FET length probes. The bars in the scatter plots **f**, **g**, **i**, **j** indicate the maximum amplitude achieved by probes with a given size and geometry.

DISTRIBUTION A: Distribution approved for public release.

Multiplexed nanoscale circuits for single/muli-cell recording.[37] Furthermore, the small size and consequent proximity of U-NWFET that can be deterministically fabricated using our nanocombing method enable us to construct unique nanodevice/cell circuits and enables unique multiplexed measurements either within a single cell or between multiple cells. Nanodevice elements can be designed either to measure either multisite IC signals within a single cell (**Fig. 30ai**), IC/EC action potentials from the single cell (**Fig. 30aii**) and propagation of action potentials in cell networks (**Fig. 30aiii**). We show that our system can simultaneously measure electrical signal from two different sites in a DRG neuron soma (**Fig. 30b**) Additionally, by modulating the design of our probes we can simultaneously measure the intracellular and extracellular electrical signal from a single HiPSC-CM (**Fig. 30c**). Finally, our system demonstrates the potential for multiplexed intracellular measurements where we show capability to simultaneously achieve multiple measurements inside the same cell as well as from different cells in a sheet of HiPSC-CM (**Fig. 30d**). Multiplexed measurements made possible by our rational design of nanoscale circuit elements on our U-NWFET platform allows us to explore subcellular potential differences within cells as well as interactions between neighboring cells.

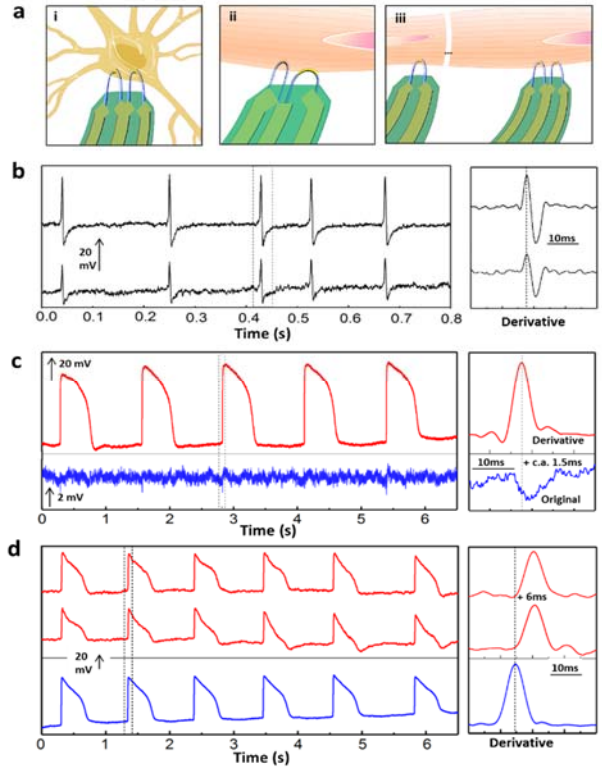

Fig. 30. Multiplexed electrophysiological recording by U-NWFET probes. a, Schematics of (**i**) simultaneous multi-site IC recording from single neuron by paired U-NWFETs on one probe arm, (**ii**) simultaneous IC/EC recording from one cell by paired U-NWFETs on one probe arm, and (**iii**) multiplexed IC recording from different cells by U-NWFETs on different probe arms. **b**, Left, simultaneous IC recording from one DRG neuron by two ca. 50 nm FETs with 0.75 µm ROC on one probe arm with a 2 µm separation. Right, the derivative of dashed block marked region. The vertical dashed guiding line indicates the time point of the first action potential. No time delay is observed. **c**, Left, simultaneous IC/EC recording from one HiPSC-CM by one ca. 50 nm FET with 0.75µm ROC and one ca. 2.0 µm FET with 1.5 µm ROC on one probe arm with 2 µm separation. Right, the derivative of IC signal (red) and original EC signal (blue) with ca. 1 ms delay. **d**, Left, multiplexed IC recording from two HiPSC-CMs by one paired U-NWFET probe and one single U-NWFET probe. Right, the derivative of marked region. The two probe arms are fabricated at a distance of 350 µm from one another.

DISTRIBUTION A: Distribution approved for public release.

References

1. Zhang A; Lieber CM (2015) *Chem Rev* **116**:215-57
2. Tian B; Cohen-Karni T; Qing Q; Duan X; Xie P; Lieber CM (2010) *Science* **329**:830-4
3. Xie C; Lin Z; Hanson L; Cui Y; Cui B (2012) *Nat Nanotechnol* **7**:185-90
4. Qing Q; Jiang Z; Xu L; Gao R; Mai L; Lieber CM (2014) *Nat Nanotechnol* **9**:142-7
5. Robinson JT; Jorgolli M; Shalek AK; Yoon M-H; Gerner RS; Park H (2012) *Nat Nanotechnol* **7**:180-4
6. Almquist BD; Melosh NA (2010) *Proc Natl Acad Sci USA* **107**:5815-20
7. Xie X; Xu AM; Angle MR;Tayebi N; Verma P; Melosh NA (2013) *Nano Lett* **13**:6002-8
8. Shalek AK; Robinson JT; Karp ES; Lee JS; Ahn D-R; Yoon M-H *et al* (2010) *Proc Natl Acad Sci USA* **107**:1870-5
9. Hanson L; Lin ZC; Xie C; Cui Y; Cui B (2012) *Nano Lett* **12**:5815-20.
10. Aalipour A; Xu AM; Leal-Ortiz S; Garner CC; Melosh NA (2014) *Langmuir* **30**:12362-7.
11. Frankel AD; Pabo CO (1988) *Cell* **55**:1189-93
12. Polyakov V; Sharma V; Dahlheimer JL; Pica CM; Luker GD; Piwnica-Worms D (2000) *Bioconjug Chem* **11**: 762-71
13. Astriab-Fisher A; Sergueev D; Fisher M; Shaw BR; Juliano R (2002) *Pharmaceut Res* **19**:744-54.
14. Moschos SA; Jones SW; Perry MM; Williams AE; Erjefalt JS; Turner JJ *et al* (2007) *Bioconjug Chem* **18**:1450-9
15. Schwarze SR; Ho A; Vocero-Akbani A; Downdy SF (1999) *Science* **285**:1569-72
16. Wadia JS; Stan RV; Dowdy SF (2004) *Nat Med* **10**:310-5
17. Mao Z; Wan L; Hu L; Ma L; Gao C (2010) *Colloids Surf B Biointerfaces* **75**:432-40
18. Morales AM; Lieber CM (1998) *Science* **279**:208-11
19. Lee JH; Zhang A; You SS; Lieber CM (2016) *Nano Lett* **16**:1509-13
20. Russell WC (2000) *J Gen Virol* **81**:2573-604
21. Karra D; Dahm R (2010) *J Neurosci* **30**:6171-7
22. Ambrosi CM; Boyle PM; Chen K; Trayanova NA; Entcheva E (2015) *Sci Rep* **5**:16
23. O'Riordan CR; Lachapelle A; Delgado C; Parkes V; Wadsworth SC; Smith AE; Francis GE (1999) *Hum Gene Ther* **10**:1349-58
24. Tian B; Xie P; Kempa TJ; Bell DC; Lieber CM (2009) *Nat Nanotechnol* **4**:824-9
25. Ozel T; Zhang BA; Gao R; Day RW; Lieber CM; Nocera DG (2017) *Nano Lett* **17**:4502-7. Highlighted on NanotechWeb: http://nanotechweb.org/cws/article/tech/69207.
26. Boehler J; Asplund M (2015) *Biomed Mater Res A* **103A**:1200-7
27. Jiang Z; Qing Q; Xie P; Gao R; Lieber CM (2012) *Nano Lett* **12**:1711-6.
28. Waddell PJ; Lawson SN (1990) *Neuroscience* **36**:811-22
29. Renganathan M; Cummins TR; Waxman SG (2001) *J Neurophysiol* **86**:629-40
30. Lin Q; Huang Q; Li C; Bao C; Liu Z; Li F; Zhu L (2010) *J Am Chem Soc* **132**:10645-57
31. Rim HP; Min KH; Lee HJ; Jeong SY; Lee SC (2011) *Angew Chem Int Ed* **50**:8853-7
32. Hakeem A; Duan R; Zahid F; Dong C; Wang B; Hong F *et al* (2014) *Chem Commun* **50**:13268-72
33. Walcarius A; Sibottier E; Etienne M; Ghanbaja J (2007) *Nat Mater* **6**:602-9
34. Sadki S; Schottland P; Brodie N; Sabouraud G (2000) *Chem Soc Rev* **29**:283-93
35. Vazquez E; Dewitt DM; Hammond PT; Lynn DM (2002) *J Am Soc Chem* **124**:13992-3

DISTRIBUTION A: Distribution approved for public release.

36. Ozel T; Hernandez E; Mutlugun E; Akin O; Nizamoglu S; Ozel O *et al* (2013) *Nano Lett* **13**:3065-72
37. Zhao YL; You S; Zhang A; Lee J; Huang J; Lieber CM. In preparation for submission to *Nat Nanotechnol*
38. Zhao YL; Yao J; Xu L; Mankin MN; Zhu Y; Wu H *et al* (2016) *Nano Lett* **16**:2644-50
39. Wu Y; Xiang J; Yang C; Lu W; Lieber CM (2004) *Nature* **430**:61-5

DISTRIBUTION A: Distribution approved for public release.